Lab on a Chip

PERSPECTIVE

View Article Online
View Journal | View Issue

Cite this: *Lab Chip*, 2023, **23**, 1389

Design of functional nanoparticles by microfluidic platforms as advanced drug delivery systems for cancer therapy

Antonio Fabozzi,[ab] Francesca Della Sala,[a] Mario di Gennaro,[ad] Marco Barretta,[a] Gennaro Longobardo,[ac] Nicola Solimando,[b] Maurizio Pagliuca[b] and Assunta Borzacchiello *[a]

Received 5th October 2022,
Accepted 28th November 2022

DOI: 10.1039/d2lc00933a

rsc.li/loc

Nanoparticle systems are functional carriers that can be used in the cancer therapy field for the delivery of a variety of hydrophobic and/or hydrophilic drugs. Recently, the advent of microfluidic platforms represents an advanced approach to the development of new nanoparticle-based drug delivery systems. Particularly, microfluidics can simplify the design of new nanoparticle-based systems with tunable physicochemical properties such as size, size distribution and morphology, ensuring high batch-to-batch reproducibility and consequently, an enhanced therapeutic effect *in vitro* and *in vivo*. In this perspective, we present accurate state-of-the-art microfluidic platforms focusing on the fabrication of polymer-based, lipid-based, lipid/polymer-based, inorganic-based and metal-based nanoparticles for biomedical applications.

1. Introduction

In the last few decades, functional structured nanoparticles (NPs) have attracted significant attention in the biomedical field thanks to their use as vehicles for the controlled delivery of different types of drugs.[1,2] The therapeutic efficacy of NPs is strictly connected to their physicochemical properties such as size and morphology; however, to obtain NPs of the desired size and shape with high batch-to-batch reproducibility remains technically challenging in the conventional synthetic batch

[a] *Institute for Polymers, Composites and Biomaterials, National Research Council, IPCB-CNR, Naples, Italy. E-mail: bassunta@unina.it*
[b] *ALTERGON ITALIA S.r.l., Zona Industriale ASI – 83040 Morra De Sanctis (AV), Italy*
[c] *Department of Chemical, Materials and Industrial Engineering, University of Naples Federico II, P. le Tecchio 80, 80125 Napoli, Italy*
[d] *Department of Environmental, Biological and Pharmaceutical Sciences and Technologies (DiSTABiF), University of Campania "L. Vanvitelli", 81100 Caserta, Italy*

Antonio Fabozzi

Dr. Antonio Fabozzi is a researcher at Altergon ITALIA Srl. He received his master's degree and then PhD degree in Chemical Sciences from the University of Naples "Federico II". He currently works in collaboration between the Institute of Polymers, Composites and Biomaterials (IPCB) of National Research Council (CNR) of Naples (Italy) and Altergon ITALIA Srl. His research interests are focused on the preparation of polymer-based nanomaterials by means of microfluidics and their physicochemical characterization for the release of active principles in the drug delivery field.

Francesca Della Sala

Dr. Francesca Della Sala obtained her master's degree in Medical Biotechnology from the University of Naples "Federico II", and then obtained her PhD degree in Biomolecular Sciences from the University of Campania "Luigi Vanvitelli". She currently works as a researcher at the Institute of Polymers, Composites and Biomaterials (IPCB) of National Research Council (CNR) of Italy. Her research interests are focused on biomaterials for tissue engineering and drug delivery application. In particular, she is interested in the study of nano–micro particles for targeted delivery and innovative polymeric substrates for regenerative medicine and cell delivery.

methods.[3,4] These features are the key points for the treatment of many forms of cancer. In particular, NPs can increase the drug concentration in cancer cells and help to overcome some limitations of conventional chemotherapy such as the low specificity to cancer cells and the toxic effects on healthy cells.[5,6] NPs can take advantage of the enhanced permeability and retention effect (EPR) that facilitates the NP accumulation into cells and tissues of solid tumors.[7,8] The EPR effect is generally displayed by tumor vessels, which show some characteristics such as an anomalous rate of growth, a disordered vascular architecture and high permeability.[8,9] Unfortunately, the EPR efficacy/efficiency is limited by some drawbacks such as a possible shortage of NP cell uptake, an undesired release of the drug before the NPs are internalized and a low percentage of the administered dose.[10] A possible strategy to overcome these limitations is aimed at providing the NPs with active targeting moieties by means of appropriate modifications of NP surfaces such as nucleic acids,[11,12] antibodies,[13] proteins,[14] and folate.[15] Indeed, functionalized NPs can be recognized and subsequently bind tumor cells and can even be internalized *via* receptor-mediated endocytosis.[15,16] However not all modifications of the NP surface represent an effective strategy to overcome the limitations of EPR, for instance recently, folic acid-functionalized liposomes do not enhance the distribution of liposomes in FR-α-overexpressed tumors.[17] For all these reasons, the NP fabrication methods represent an important tool for the reproducibility of biological assays. In particular, there are a variety of NP synthetic conventional methods such as nanoprecipitation,[18] solvent evaporation,[19,20] microemulsions,[21] sol–gel,[22,23] emulsion polymerization,[24] layer-by-layer self-assembly,[25] thin-film hydration,[26] bulk mixing by extrusion,[27] pipette mixing,[28] electrodeposition and thermal decomposition.[29,30] In these methods, the formation of the NPs can be divided into three stages, a) nucleation, b) growth and c)

Mario di Gennaro

Mario di Gennaro received his master's degree in Science and Technologies of Industrial Chemistry from the University of Naples "Federico II". Currently, he is a PhD student in Biomolecular Sciences at the University of Campania "Luigi Vanvitelli" under the supervision of Dr. Ing. Assunta Borzacchiello. His current research interests are focused on the preparation and physical, chemical and rheological characterization of polysaccharide-based nanostructured materials for the release of active principles in the biomedical applications field.

Marco Barretta

Marco Barretta received his master's degree in Materials Engineering cum laude from the University of Naples "Federico II". Currently, he is a post graduate student at IPCB-National Research Council of Italy under the supervision of Dr. Ing. Assunta Borzacchiello. His current research is based on the preparation and physicochemical characterization of polysaccharide-based nanostructured materials for the release of active principles in the biomedical applications field.

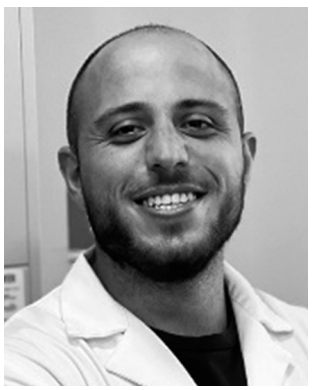

Gennaro Longobardo

Gennaro Longobardo obtained his master's degree in Materials Engineering cum laude from the University of Naples "Federico II". Currently, he is a PhD student in "Industrial Products and Process Engineering" at the University of Naples "Federico II" under the supervision of Dr. Ing. Assunta Borzacchiello. His current research interests are focused on the preparation and characterization of biomaterials for tissue engineering and controlled drug release.

Nicola Solimando

Dr. Nicola Solimando received his master's degree in Biology cum laude from University la Sapienza (Rome) in 1995 and he did research activity as a research fellow at the same university in the field of genetic engineering and chemistry of fermentation processes. Since 2010 he has been a Production and R&D manager at Altergon ITALIA S.r.l and his research interests are related to fermentation plants of injectable grade polysaccharides and development of microneedles and microfluidics technology on the pilot scale. During more than 20 years of working in pharmaceutical companies, he has acquired knowledge in project management and technology transfer.

Table 1 Examples of NPs fabricated by microfluidics for biomedical applications

Nanomaterials			Microfluidic mechanisms	Active principles	Drug encapsulation efficiency (%)	Ref.
Polymer-based NPs	Natural polymers	L/CS	Self-assembly	Docetaxel/curcumin	95/99	85
		HA/CS	Nanoprecipitation	Everolimus	88	and 86
	Synthetic polymers	PLGA	Emulsification	5-Fluorouracil	95	87
		PTMC-PCL/PEG-b-PDLLA	Nanoprecipitation	Doxorubicin	51	and 88
Lipid-based NPs	Lipid NPs	C12–200/DOPE cholesterol lipid–PEG	Self-assembly	siRNA and/or mRNA	83/81	98
		Tf-lipid NPs	Self-assembly	siRNA	78	99
	Solid lipid NPs	Cetyl palmitate	Nanoprecipitation	Paclitaxel Sorafenib	54 79	119
Lipid/polymer-based NPs		PLGA/DSPE-PEG2000	Nanoprecipitation	Sorafenib	88–95	125
Core–shell NPs		PCL-PEI/cholesterol, DSPE-PEG2000, DOPE	Three step self-assembly	siRNA	79–98	26
		PLGA-lipid/PEG	Nanoprecipitation	—	—	129
Inorganic-based NPs	Mesoporous silica NPs	Dox-loaded/MSN/PTX/polystyrene sulfonate	Nanoprecipitation	Doxorubicin/paclitaxel	70/94	141
	Ellipsoidal mesoporous silica	Dox-loaded EMSNs	Nanoprecipitation	Doxorubicin	70	142
	Quantum dots	AIE QDs Dspe-PEG2k	Nanoprecipitation	—	—	146
	MOF	BioZIF-8	Self-assembly	siRNA/BSA/DOX	53/59/47	149
Metal-based NPs	Cu-based NPs	BSA/$Cu(DDC)_2$MONs	Nanoprecipitation	$Cu(DDC)_2$	66–95	162
	Polymer–metal NPs	Chitosan/silver NPs	Emulsion	*Calotropis procera* extract	77	163

aggregation, which occur concurrently leading to some differences, in terms of physicochemical properties, from batch-to-batch of synthesized NPs.[31] The inability to control the physicochemical properties of each synthetic batch of NPs leads to low reproducibility of both *in vitro* and consequently *in vivo* biological tests.[32] The new continuous-flow microfluidic systems are largely investigated for their properties such as rapid mass transfer, precise control, large reaction interfaces, and mixing efficacy.[33] In particular, the nucleation, growth, and aggregation steps of the NPs can be separated as a function of distance from the position where the solution occurs in order to achieve absolute control of the physicochemical properties, including particle size and morphology.[34,35] Thus, compared to conventional methods, the microfluidic technique allows for overcoming all limitations for the production of NPs, increasing the reproducibility of each synthetic batch and favoring the

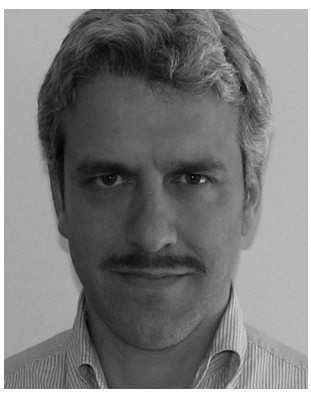

Maurizio Pagliuca

Dr. Maurizio Pagliuca earned his master's degree in Biological Sciences cum laude from the University of Naples "Federico II". From 2003 to 2009 he worked as a Site & Technical Director at Altergon Italia, and since 2009 he has held the office of Chief Operating Officer – Technical Director at Altergon Italia. With over 30 years in the pharmaceutical industry, Dr. Pagliuca's experience includes the biotech production of ultrapure hyaluronate and ultrapure GAGs, and the research and development and the industrial scale up of customized drug delivery systems.

Assunta Borzacchiello

Assunta Borzacchiello earned her master's degree in Chemical Engineering cum laude (1994) and PhD degree in Material Technologies (1998) from the University of Naples "Federico II". She was a Research Scientist at QMWC University of London (1996) and at the University of Connecticut, USA (1997). She was a Professor of Biomaterials at the University of Naples "Federico II" from 2002–2011. She was a Visiting Professor at McGill University, Canada (2018, 2019). She is currently a Senior Scientist at IPCB-National Research Council of Italy. The Borzacchiello group is currently focusing on biomaterials for tissue engineering and drug delivery applications, microfluidic techniques for biomedical applications and rheology and microrheology of complex fluids.

industrial scale-up, and represents a new strategy capable of overcoming challenges in the clinical field of NP drug carriers[36] (Table 1). In this perspective, we discuss and highlight the developments and the applications of NPs fabricated by microfluidics as advanced delivery systems focusing on: a) polymer-based NPs, b) lipid-based NPs, c) lipid/polymer-based NPs, d) inorganic-based nanoparticles, and e) metal-based nanoparticles.

2. Flow systems for nanoparticle synthesis

Nowadays, NPs are synthesized by means of traditional methods from the corresponding precursors employing different approaches, described above, in which it is difficult to control their physicochemical properties.[37] In the last decade, the microfluidic flow systems employed for NP fabrication have been largely studied due to their advantages such as high control of physicochemical properties and high reproducibility of synthetic batches.[38,39] The microfluidic flow control systems depend on the Reynolds number (Re) and the Péclet number (Pe) that allow high levels of control over the production of NPs. Re describes the flow properties, as a ratio between inertial and viscous forces, and can be calculated by eqn (1).

$$\mathrm{Re} = \frac{\rho v L}{\mu} \tag{1}$$

where ρ represents the density of the fluid, v is the average velocity of the fluid, L represents the diameter of the pipe, and μ is the viscosity of the fluid.[40,41] For a microfluidic setup, a high Re number can be obtained by increasing the flow rate and/or the density of the liquids or by decreasing the viscosity of the fluids. However, a Re number >2300 produces a turbulent flow with random streamlines (Fig. 1a).[42] In contrast, a Re number <2000 produces a laminar flow with distinct streamlines parallel to the fluid direction in order to achieve high control of monodisperse droplets (Fig. 1b).[43]

The Pe number describes the diffusion, based on the random thermal motion of molecules in their surrounding environment, and convection phenomena of the molecules, based on the movement of molecules from the bulk motion of a fluid.[44] The Pe number range, 250–2500, shows an upper limit that is strictly connected to the Re constraint[45] and can be calculated by eqn (2).

$$\mathrm{Pe} = \frac{U_a H}{D} \tag{2}$$

where U_a represents the average velocity of the flow, H is related to the length of the system, and D represents the mass diffusion coefficient of the NPs. In a microfluidic droplet, the transport of molecules is slow and it occurs mostly by diffusion because of the laminar flow and small volume.[41] For this reason, the transport of molecules from the dispersed to the continuous phase is minimized, and consequently, a high drug encapsulation efficiency is obtained.[42,44] The microfluidic devices can be categorized into two classes, single-phase continuous (SPCF) flow and multi-phase flow microfluidic systems (MPF) even known as segmented flow.

2.1. Microfluidic systems based on single-phase continuous flow

The SPCF system is the most commonly employed in microfluidics because it is a homogeneous system that provides simplicity and versatility of a variety of features such as control of the flow, reaction time, temperature and reagents (Scheme 1a). In particular, the fabrication of NPs in SPCF microfluidic systems can be carried out using single or multiple miscible solvents and the reagents are mixed by means of diffusion in laminar flows.[46,47] For the SPCF microfluidic systems, the main mixing mechanism is based on molecular interdiffusion obtained by means of laminar flows.[48] Indeed, most single-phase microfluidic mixers are designed to operate with a Reynolds number <2000, in order to achieve the absence of turbulent flows.[49]

The mixing time (τ_{mix}) quadratically depends on the channel width and the flow rate ratio of the miscible flows and can be estimated by the following equation:

$$\tau_{mix} \sim \frac{w_f^2}{4D} \approx \frac{w^2}{9D}\frac{1}{(1+1/R)^2} \tag{3}$$

where D is the diffusivity of the reagents, w_f is the width of the focused stream, w is the channel width, and R is the ratio of the flow rate between the reagent stream and the total flow rate of the solvent.[50] In order to improve the mixing performances, a transverse component of the flow can be

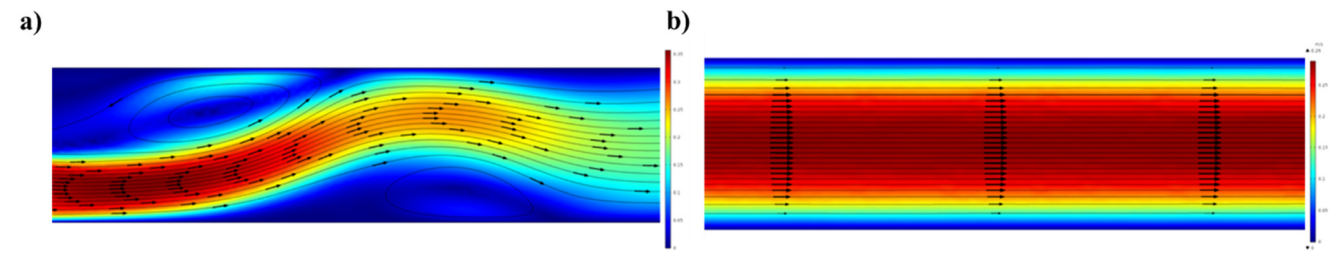

Fig. 1 Schematic illustration of different types of representative flow patterns in FEM microchannels simulated using COMSOL Multiphysics® (velocity magnitude (m/s)); the arrows represent the streamline velocity field: a) turbulent flow and b) laminar flow.

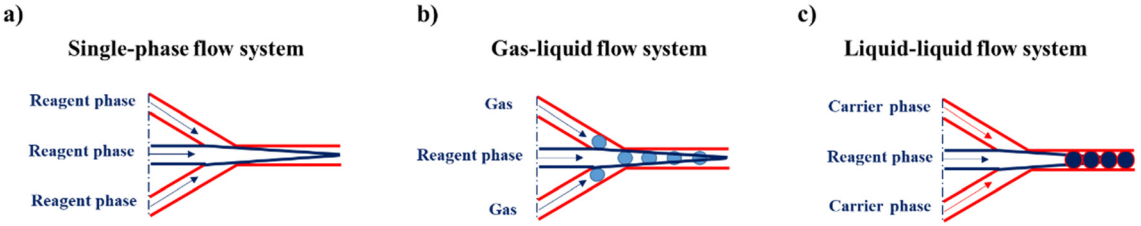

Scheme 1 Representative illustration of a) a single-phase flow system, b) a gas–liquid flow system and c) a liquid–liquid-flow system.

incorporated and chaotic advancement can be activated in the microchannels through repeated cycles based on the stretching and bending of the flows. This can be achieved through the use of a staggered herringbone mixer in order to obtain exponentially thin flow, leading to the exponential growth of the interface between two fluids to obtain rapid mixing.[51] Furthermore, the micrometric dimensions of a microchannel permit the reduction of the mixing time to milliseconds during the nucleation stage in the NP synthesis.[52] Moreover, the SPCF system offers the advantage of modifications during NP synthesis by adding new reagents during the reaction.[53] From an industrial point of view, the SPCF system can be scalable through multiple parallel reactions in order to synthesize a large amount of NPs.[54]

2.2. Microfluidic systems based on multiphase flow

MPF microfluidic-based systems are composed of two isolated phases of two or more immiscible fluid phases, in which the addition of a new phase activates a recirculation motion generating the stretching and bending of a solution that improves the mixing efficiency.[55] Furthermore, the MPF synthesis strategy offers some advantages such as reducing the deviation of the residence time, because the reactions occur in well-defined droplets, and the reduced risk of channel clogging thanks to the minimization of the direct contact of the liquid with the microchannel.[56] Moreover, MPF synthesis can be split into two sub-classes: gas–liquid flows (GlF) (Scheme 1b) and liquid–liquid flows (LlF) (Scheme 1c). The LlF consists of two phases, such as water-in-oil or oil-in-water dispersions, in which surfactants can be added in order to inhibit the coalescence of the dispersed droplets.[57–59] The morphology of the droplets is strictly connected to two parameters: a) the flow rate and b) the chip design.[60,61] Thanks to the appropriate mixing efficacy, mass transfer and quick heat in LlF systems, NPs with a variety of shapes can be synthesized in these systems.[62,63] The reacting solutions are encapsulated within liquid droplets, preventing contamination and channel clogging, leading to the higher reproducibility of NP synthesis.[64] The GlF systems are composed of a bubbly flow dispersed in a continuous liquid phase. The employment of a gas phase can significantly enhance the mixing efficacy thanks to the creation of recirculation.[65,66] One of the most interesting characteristics of gas–liquid flow reactors is based on the separation of the gas from the liquid to achieve the desired NPs. Unfortunately, in the GlF systems, possible clogging can be obtained which can be avoided with the employment of liquid–liquid flow reactors.[67]

The microfluidic industrial scale-up technologies offer the opportunity for the fabrication on a large scale of NP-based systems widely used for cancer treatments.[68] The high-throughput fabrication of NPs with control of physicochemical properties such as size and shape is one of the critical points for their effective biomedical applications.[69] In particular, a microfluidic industrial scale-up device can be composed of thousands of micromechanical valves that permit the production of NPs in an automated device.[70] Generally, two strategic approaches for the industrial scale-up of microfluidic drop generators have been developed and are based on a single chip in which there is an integration based on multiple parallel drop generation units[71] or multiple chips each containing parallel drop generation units as described elsewhere.[72] In particular, the two main microfluidic device configurations used for the industrial scale-up, employed to dispense fluids from a single manifold into multiple parallel drop generation units, are the tree-type and ladder-type.[73,74] Although, the ladder-type configuration shows some advantages such as small random variation in the channel size and compact design, even if a clogging issue can inhibit the NP production,[73] the tree-type is more energy efficient.[74] For these reasons, a combination of two configurations based on multiple chips offers the possibility of synthesizing NPs even if a clogging issue can be detected. Although microfluidic technology is widely used for the synthesis of NPs, its industrial applicability is still an ongoing challenge due to the eventual clogging of both microchannels and microchips. For this reason, some enhancements need to be applied for the production of tons of nanomaterials. Moreover, a microfluidic method for both small and large-scale NP production is the use of a NanoAssemblr™. The microfluidic NanoAssemblr™ platform is employed for the rapid and controlled synthesis of a variety of NPs such as polymer-based[75] NPs and polymer–lipid-based NPs in the nanomedicine field.[76] In particular, the microfluidic mixer is designed to achieve optimization for precise control of the physicochemical properties requiring nanoparticle self-assembly in the nanomedicine field.[77,78] NPs are synthesized on fast time scales minimizing the process variability. The NanoAssemblr™ synthesizes NPs in <1 min and kilograms of formulations per day; in particular, NPs developed by means of the NanoAssemblr™ are scaled

without employing a microfluidic mixer parallelization and continuous flow pumping system. A single microfluidic mixer can work at $N \times 24$ mL min^{-1} and can generate NPs higher than 24 mL min^{-1} of *N*-parallelized mixers.[79]

3. Application of nanoparticles fabricated by microfluidics as delivery systems

3.1. Polymer-based nanoparticles

Polymer-based NPs, composed of natural and synthetic polymers, have been widely fabricated by means of microfluidics and investigated in the drug delivery field thanks to their unique properties such as biodegradability and biocompatibility.[80–82] The advantages of microfluidic fabrication of polymer-based NPs are based on the enhancement of the control of physicochemical properties such as size, size distribution, and morphologies.[83,84] Some examples, reported in the literature in the last two years, based on polymeric NPs have been selected and described as follows.

Docetaxel (Dtx) and curcumin (Cur) loaded lignin/chitosan (L/CS) NPs were fabricated in a simple and scalable microfluidic system for flash nanoprecipitation to test their delivery potential and cytotoxicity. Briefly, L, used as the organic phase, and CS, solubilized in 0.1 M acetic acid, used as the aqueous phase, solutions were rapidly mixed in a torus-shaped mixing chamber and quickly co-assembled into L/CS NPs in a valve-assisted mixer equipped with a medium-pressure constant flow pump (Fig. 2).

The hydrophobic anticancer drugs such as Cur or Dtx were solubilized in the organic phase of L. The morphological analysis of L/CS NPs showed an average particle size of about 180 nm. The drug release amounts in acidic solutions simulating the tumor environment were 51% for Dtx-L/CS NPs and 50% for Cur-L/CS NPs, respectively, which were higher than the release amounts at pH 7.4, showing a killing effect, in both cases, on HeLa cells. Furthermore, L/CS NPs exhibited low cytotoxicity, demonstrating good cell compatibility.[85] The microfluidic platform was employed for the one-pot fabrication of hyaluronic acid–chitosan (HA–CS) NPs, based on the polyelectrolytic interactions between CS and HA. Briefly, a staggered herringbone micromixer was used for the fabrication of HA–CS NPs in which a CS aqueous solution and a mixture composed of HA and sodium tripolyphosphate (TPP) aqueous solutions were injected into different microchannels (Fig. 3a).

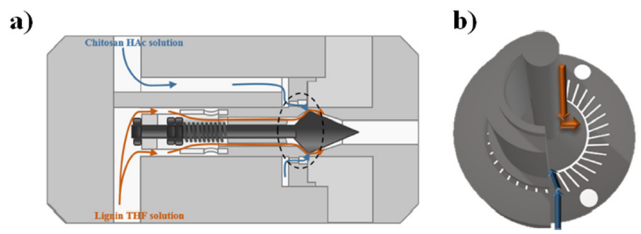

Fig. 2 (a) Schematic representation of the valve-assisted mixer structure. (b) Fluid guidance *via* the mixing plate. Reprinted with permission from ref. 85. Copyright 2021. American Chemical Society.

The microfluidic on-chip fabrication allowed the fabrication of HA/CS NPs with controlled size and appropriate for both loco-regional, 350 nm, and parenteral, 117 nm, administration. Everolimus (EV), a water-insoluble anticancer drug able to reduce angiogenesis and promote apoptosis, was encapsulated in the HA/CS NPs. *In vitro* cellular uptake tests, carried out on human mesenchymal stem cells, demonstrated a blockage of the CD44 receptor by the primary anti-CD44 antibody compared to CS-based NPs thanks to the high selectivity of HA/CS NPs with CD44 (Fig. 3b).[86] Among all synthetic polymers, poly(D,L-lactide-*co*-glycolide) (PLGA) based NPs, fabricated by means of microfluidic methods, are the most employed in the drug delivery field. Indeed, during the NP synthetic process, a variety of drugs such as docetaxel, doxorubicin and curcumin can be effectively encapsulated inside the hydrophobic core composed of PLGA. An example, based on the fabrication of 5-fluorouracil (5-FU)-loaded PLGA NPs *via* the emulsification mechanism through a fork-shaped chip by means of a microfluidic technique, with diameters of ~101 nm and a drug encapsulation efficiency of ~95 for the potential use in colorectal cancer therapy, has been reported (Fig. 4a). Briefly, a mixture composed of 5-FU and poly(vinyl alcohol) was injected into the middle microchannel as a dispersed phase and PLGA solution as a continuous phase was inserted into the external microchannels.

In particular, the biological assays on the Caco2 and SW-480 colon cancer cell lines demonstrate that the cell viability was decreased by increasing the exposure time of neat 5-FU and MF-fabricated PLGA NPs/5-FU (Fig. 4b). Furthermore, the flow cytometry and 4′,6-diamidino-2-phenylin-dole (DAPI) staining showed that the PLGA NPs/5-FU NPs were able to kill cancerous colon cells 1.5-fold higher than the control sample for Caco2 and SW-480 at a gradual rate and safe drug dosage.[87] A microfluidic approach was employed for the preparation of (co)polymeric and (co)polymer–tannic acid (TA) NPs in a microfluidic flow-focusing glass-capillary device by means of microfluidic-assisted nanoprecipitation for breast cancer. The water phase was composed of Milli-Q water, while the organic phase was composed of poly(ε-caprolactone) (PCL) and poly(trimethylene carbonate) (PtMc) homopolymers and (co)polymers with different proportions of comonomers which were synthesized by means of enzymatic polymerization. Besides, TA was added to the (co) polymer solution to fabricate NPs. In the flow-focusing device, the (co)polymers, with doxorubicin (DOX) and TA, dissolved in *N*-methyl-2-pyrrolidone, were delivered to the outer capillary, and the aqueous phase flowed counter-currently by means of the space among the square and inner capillary and the resulting nanosuspension was collected from the inner capillary (Fig. 5a).

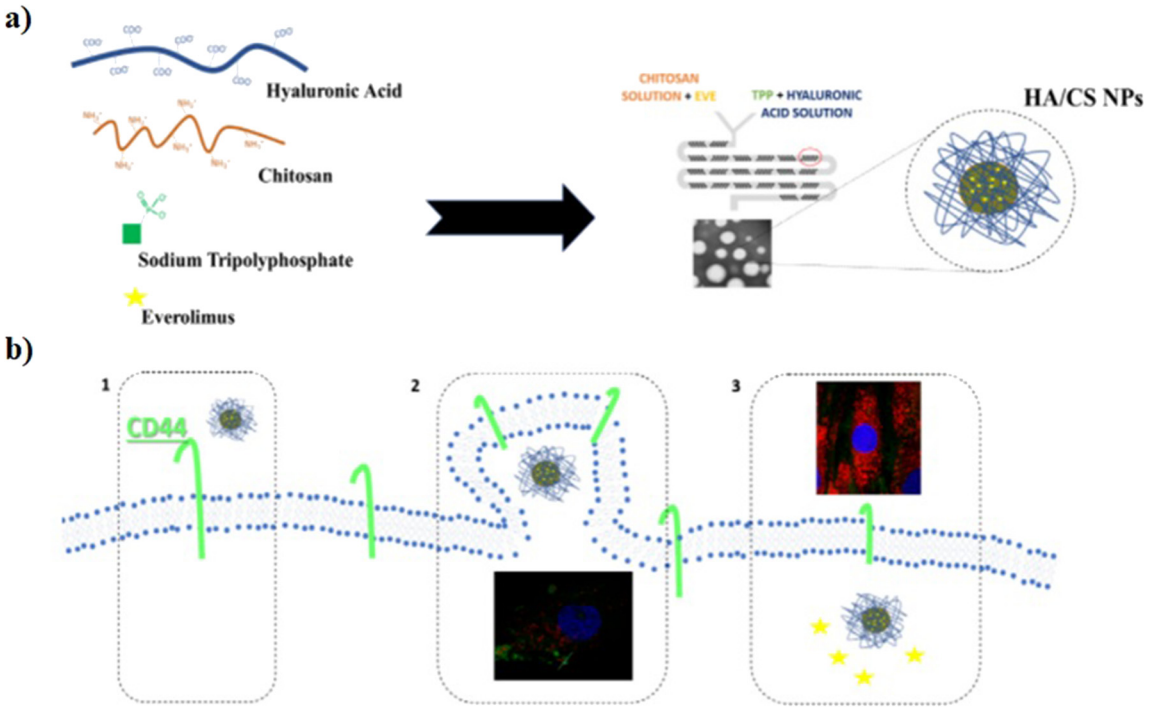

Fig. 3 a) Mechanism of HA/CS NPs in the microfluidic chip; b) ideal mechanism of action: 1) interaction between HA/CS NPs and CD44, 2) NP internalization, and 3) everolimus release. Reprinted from ref. 86.

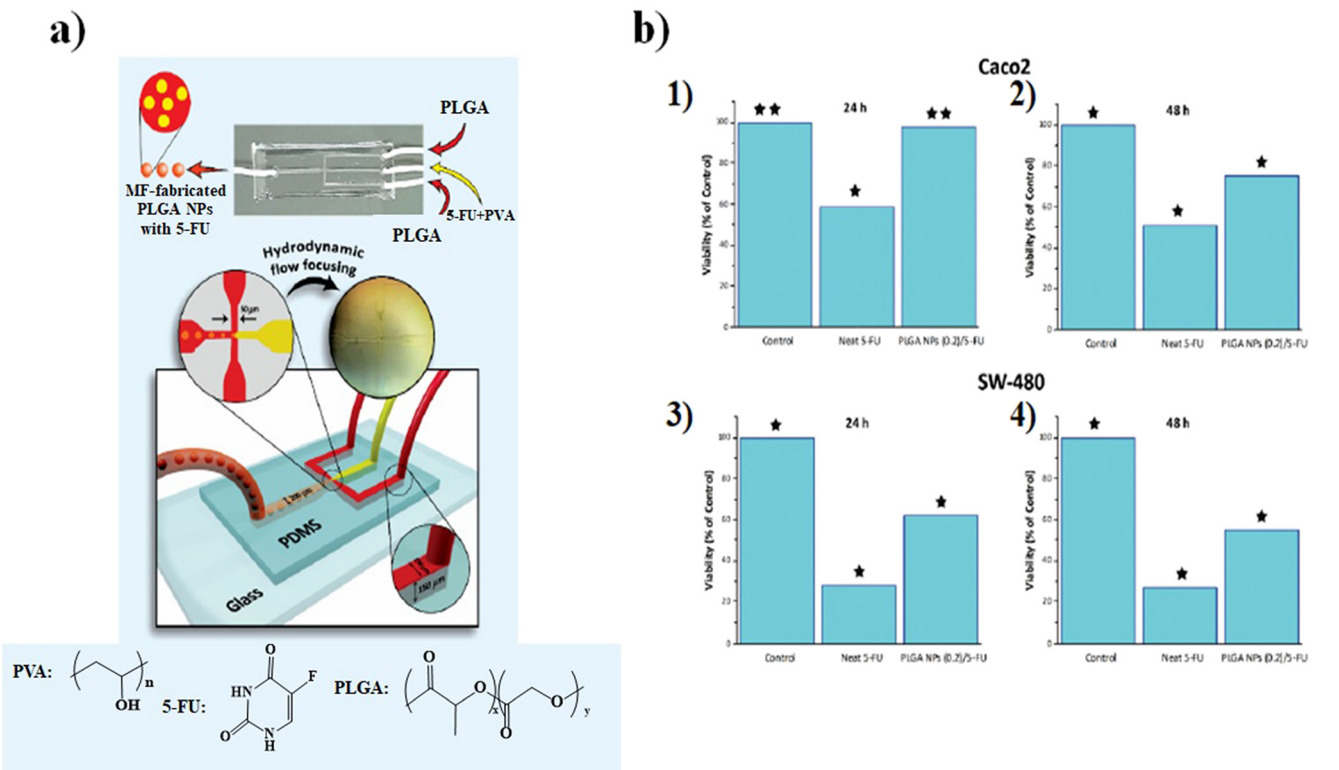

Fig. 4 a) Representation of the microfluidic chip, b) MTT cytotoxicity assay results: Caco2 (1) 24 h and (2) 48 h and SW-480 (3) 24 h and (4) 48 h. Reprinted from ref. 87.

Furthermore, poly(ethylene glycol) methyl ether-*b*-poly(D,L-lactide) (PEgmE-*b*-PDLLA) was chosen to generate a PEG corona on the resulting NPs, previously added into the organic phase during the NP fabrication (Fig. 5b). The size of NPs was set over the range of 140–230 nm by regulating both compositions and the flow rate of the phases. Furthermore, the

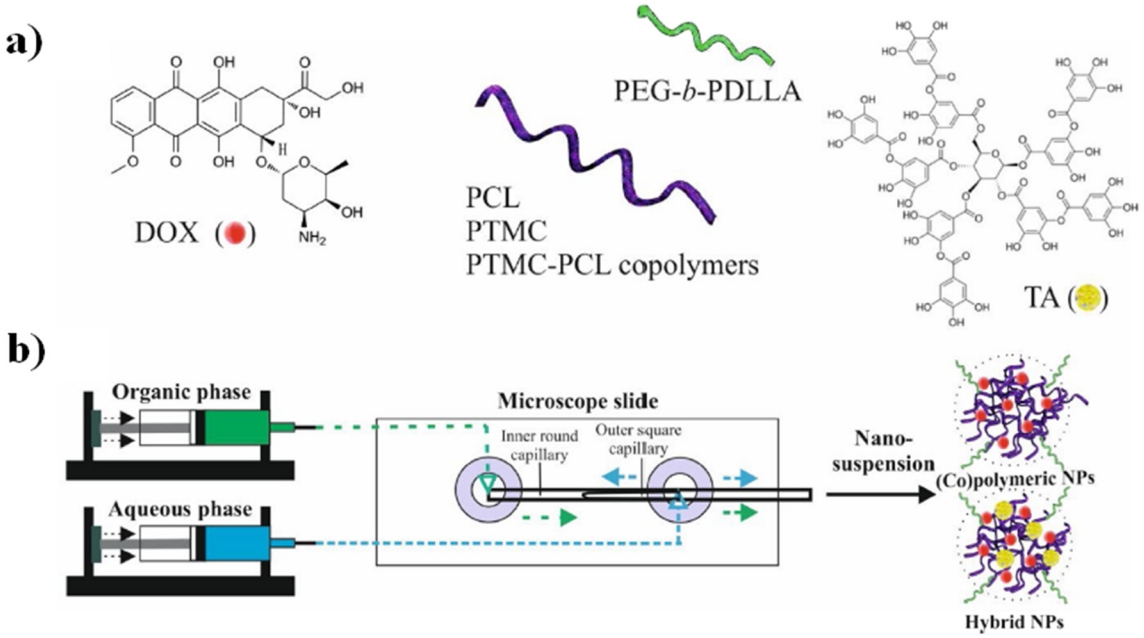

Fig. 5 a) DOX, tannic acid, and the schematic illustration of (co)polymer chemical structures. (b) Schematic representation of NP fabrication in a microfluidic device and examples of the self-assembly into NPs in water. Reprinted with permission from ref. 88. Copyright 2021 Elsevier.

drug release investigations of DOX showed that the drug release is influenced by four parameters: a) (co)polymer molecular weight, b) their composition, c) the presence of TA and d) the size of the NPs. *In vitro* tests toward breast cancer cells (MCF-7) have shown that among all formulations, the NPs composed of Dox-loaded PCL/TA show a higher efficiency to inhibit the cell proliferation of MCF-7 cells.[88] Although great efforts have been made to design new chips and synthesize new synthetic and natural polymer-based NPs, not all nanosystems are easily scalable from an industrial point of view, both because they can involve chemical modifications of the raw material and because the design of the chips cannot always be reproduced on a large scale. Furthermore, not all polymer-based NP systems exhibit high drug encapsulation efficiency. For these reasons, in the next few years, microfluidics-related research trends should be focused on the production of chemically unmodified polymer-based NPs fabricated by using a simple chip design in order to achieve a higher drug encapsulation efficiency than those fabricated previously and simple industrial scale-up.

3.2. Lipid-based nanoparticles

Lipid-based NPs, besides liposomes, have a variety of possible applications such as cosmetics, food/nutrition, nutraceuticals, drug delivery, and sustained release of active compounds and represent efficient delivery systems for nucleic acids.[89] In particular, small interfering RNAs (siRNAs), a class of double-stranded RNA molecules, typically 20–25 base pair nucleotides in length, are the most commonly investigated nucleic acids for gene therapy.[90] Gene therapy involves any procedure intended to treat or alleviate a disease by genetically modifying the cell of a patient. The siRNA acts within the RNA interference (RNAi) pathway, interfering with the expression of specific genes with complementary nucleotide sequences by destroying mRNA (messenger RNA) after transcription, preventing protein synthesis within the target cells. Thus, the appropriate design of siRNA could theoretically allow the silencing of any gene in the body, providing tremendous therapeutic potential in cancer therapy.[91] However the low transfection rates of naked RNAs, as well as their rapid degradation by serum endonucleases and anionic repulsions with cell membranes, are only some of the most challenging limitations in their delivery.[92] To overcome these limitations, RNAs are encapsulated in LNPs by the microfluidic method (MM) and bulk method (BM), in which a lipid solution in ethanol is mixed with an aqueous solution (*e.g.* acetate buffer solution) containing the nucleic acid to produce LNPs *via* self-assembly.[93] The development of specialized ionizable amino lipids has attracted scientific attention because they can be set to the delivery needs of the siRNA molecule leading to enhanced activity of LNPs–siRNA.[94,95] Furthermore, the advent of rapid-mixing methods has accelerated their commercial success and the clinical translation employment of LNPs.[96] In particular, by employing rapid-mixing methods such as a staggered herringbone mixer, an encapsulation efficiency, about ~100%, and a single and uniform population of LNPs could be achieved from the lab to the industrial scale.[76,97] A new microfluidic architecture composed of ladder-designed flow resistors and staggered herringbone micromixers (SHMs) out of the parallelized microfluidic device (PMD) (Fig. 6) was developed and compared with a microfluidic single-channel device and the usual bulk mixing method to produce LNPs encapsulating either siRNA for *in vitro* screening cell lines or mRNA or siRNA for gene expression or *in vivo* gene silencing.[98]

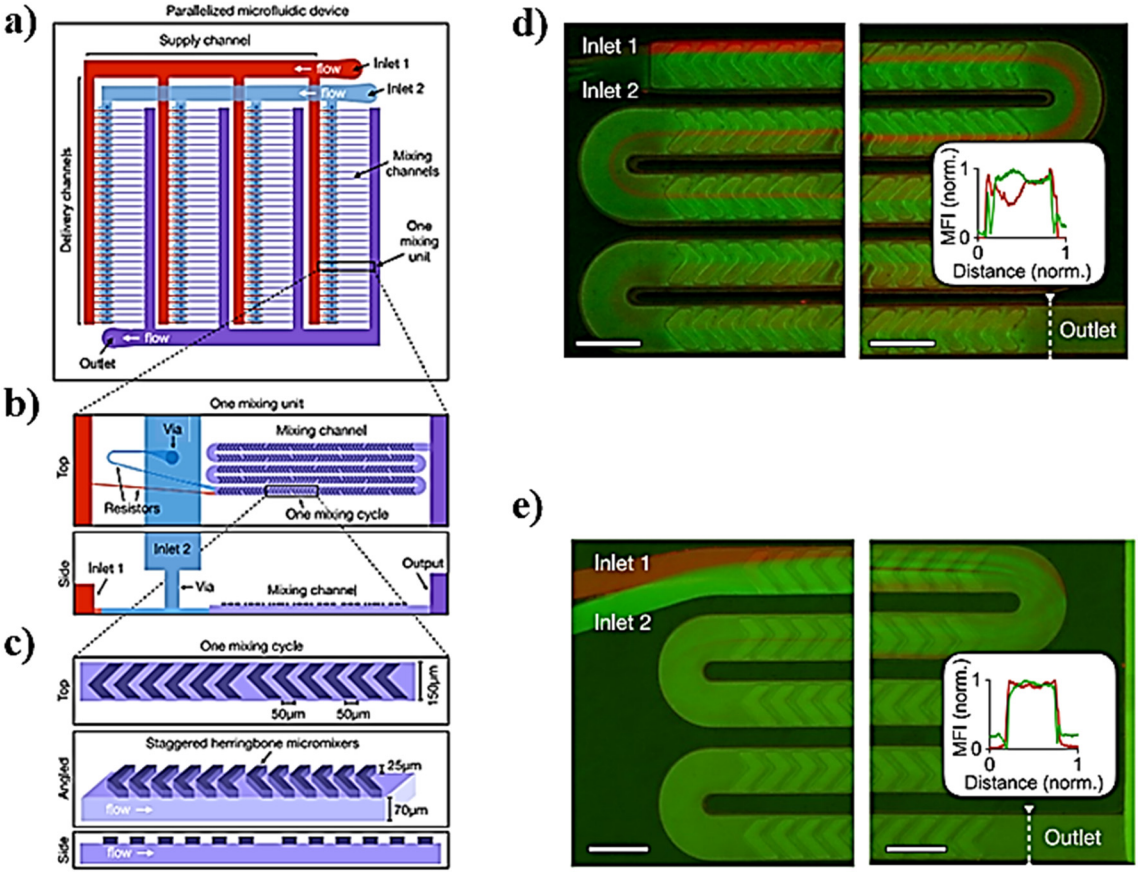

Fig. 6 a) Schematic representation of the parallelized microfluidic device (PMD) for the design of this device, consisting of an array of 4 rows of 32 SHMs, each connected to layers of channels that deliver and collect fluid from each device in the array. b) Example of an individual mixing unit from a different angle. c) Example of an individual mixing cycle constituting the mixing unit. d and e) To validate the parallelized microfluidic design, fluorescence images of mixing in channels were taken. Scale bars: 200 μm. Image adapted from ref. 98.

In particular, LNP self-assembly had to be achieved in the device and, therefore, luciferase siRNA was rapidly mixed with a solution of lipids (*i.e.* C12-200, phospholipid 1,2-dioleoyl-*sn-glycero*-3-phosphoethanolamine (DOPE), cholesterol, and lipid–PEG). Besides, mRNA LNPs were produced likewise, by mixing luciferase mRNA with the previous solution of lipids. In the end, by comparing both the MM and BM, the results showed how the PMD produced LNPs at a large scale with dimensions of ~70 nm and capable of achieving substantial *in vivo* siRNA and mRNA delivery, comparable to results obtained for a single channel microfluidic device. Li *et al.* developed transferrin-conjugated lipid NPs (Tf-LNPs) by using a staggered herringbone micromixer which were compared with those using a multi-step bulk method. Briefly, Tf–PEG–Chol was synthesized using a method described elsewhere. siRNA-loaded LNPs were fabricated by both the MM and BM. Lipids such as 1,2-di-*O*-octadecenyl-3-trimethylammoniumpropane (DOTMA), 1,2-dioceyloxy-3-dimethylaminopropane (DODMA), phosphatidylcholine (PC), cholesterol (Chol) and mPEG–Chol were dissolved in ethyl alcohol as the lipid solution, and siRNA was dissolved in HEPES-citrate buffer at pH = 4. Fig. 7 shows the microfluidic chip composed of two sides: in the first section, the internal phase was composed of lipid solution while the external phase was composed of siRNA

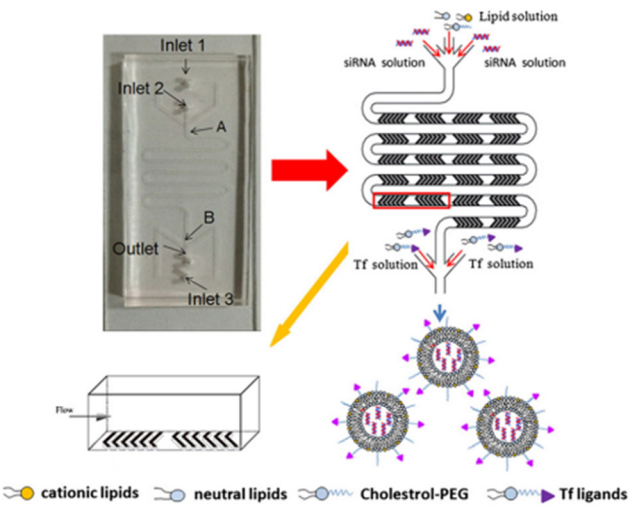

Fig. 7 Schematic representation of Tf-LNP fabrication using the staggered herringbone micromixer. Reprinted with permission from ref. 99. Copyright 2016. Elsevier.

solution in which chaotic mixing of the solutions was achieved by the staggered herringbone micromixer structure; subsequently, the second section, composed of the Y-junction with the second external phase, was composed of HEPES buffer or Tf–PEG–Chol solution.

Physicochemical characterization demonstrated that Tf-LNPs-MF showed smaller size (~132 nm) and more uniform structures compared to LNPs produced by the multi-step BM (~152 nm). Furthermore, the *in vitro* biological test on HepG-2 cells demonstrated efficient internalization of Tf-LNPs fabricated by the MM as well as greater tumor inhibition *in vivo*, achieved by injection of Tf-LNPs-siRNA by the MM and free siRNA intravenously into mice, demonstrating that the Tf-LNP MM had higher siRNA delivery efficiency both *in vitro* and *in vivo*.[99] In the last few decades, LNPs have been also commonly used in drug delivery; however, in LNPs, as well as in liquid nanoemulsions for parenteral nutrition, a controlled drug release is quite difficult to achieve, due to the small size of the carriers, as well as due to their liquid state, leading to a rapid release of the drug.[100] Thus, among colloidal systems with characteristic dimensions between 10 and 1000 nm, solid lipid nanoparticles (SLNs) were introduced at the beginning of the 90s as potential alternative carrier systems able to encapsulate with higher efficiency lipophilic drugs such as DOX,[101] ciprofloxacin,[102] tetracaine, etomidate and prednisolone.[103] Furthermore, SLNs can be used like LNPs as delivery systems for immunotherapy, gene therapy, or prophylactic vaccines, by encapsulating free nucleic acids,[104] as their electron-dense core of nucleic acid/lipid complexes can easily grant an efficient intracellular delivery of such nucleic acids.[105] SLNs can be seen as an evolution from parenteral nutrition emulsions, where the oil phase composed of a liquid lipid has been replaced with a lipid that is solid at room temperature (*e.g.* fatty acids, purified triglycerides, glyceride mixtures, *etc.*).[106] In fact, they are usually produced with a variety of lipids: from common triglycerides (*e.g.* tricaprin,[107] trilaurin[103] and tripalmitin[108]) to steroids (*e.g.* cholesterol) and to waxes (*e.g.* cetyl palmitate).[109] Moreover, SLNs take advantage of their solid core in order to maximize the drug release time through diffusion from the lipidic nucleus to the outside. Different from LNPs, a solid nucleus can prevent drugs from clearance by the reticuloendothelial system, maintaining all the benefits of the liquid nanoemulsion.[110] Eventually, SNLs have been proven to be capable of controlling/targeting drug release, improving the stability of both lipophilic and hydrophilic drugs, granting effective biodegradability and excellent biocompatibility, in addition to great ease in scaling up and sterilizing.[111,112] However, SNLs show some drawbacks, with some of them potentially vitiating their massive use: SNLs present a poor drug load capacity and a frequently occurring drug expulsion, following lipid polymorphic transition.[113] Early SNL production involved the precipitation of LNPs through bulk mixing by extrusion, pipette mixing, or other methods.[114] Generally BMs fabricate NPs with variable physicochemical and biological properties, showing a wide dimensional range, averagely above 100 nm, which are therefore incompatible with numerous tissue fenestrations, as the size influences *in vivo* biodistribution, uptake, and clearance.[93,115] Meanwhile MM-produced SLNs showed a very narrow PDI, together with generally uniform and controlled physiochemical properties thanks to the intrinsic control over small volumes flowing in the channels,[116] granting an efficient tunability of drug encapsulation, loading efficiency and release rate.[117] Besides, the microfluidic architecture can be interestingly selected or designed, in order to have an *ad hoc* reagent flow.[118,119] In a recent study, two different microfluidic devices were assembled from borosilicate glass capillaries and glass rods to produce cetyl palmitate-based SLNs.[120] In the first one, the end of the cylindrical glass capillary was tapered using a micropipette puller; in contrast, device 2 shows a three-port valve connected after device 1, in which an immiscible fluid such as air can flow to maximize mixing efficiency (Fig. 8).

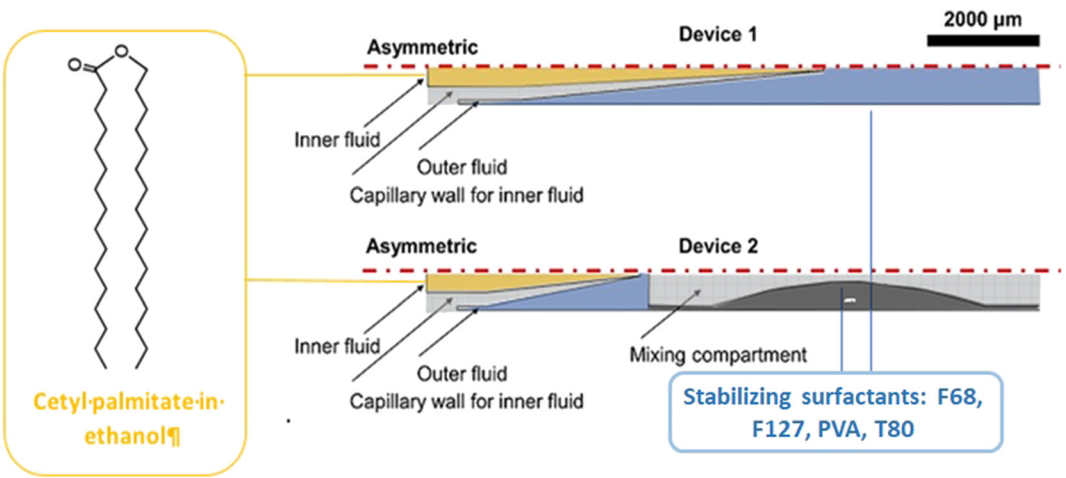

Fig. 8 Schematic representation of microfluidic devices 1 and 2. As for device 1, the outflow is collected and cooled; for device 2, the outflow is further connected to a three-port valve with continuous air pumping (mixing compartment). Image adapted from ref. 120.

Briefly, SLN nanoprecipitation with a co-flow geometry was obtained by using cetyl palmitate and DSPE-PEG as lipid inner fluid, dissolved in a 95% ethanol solution, while the outer continuous fluid consisted of an aqueous solution containing stabilizers. The effect of different parameters such as variation in the flow rate, flow speed, type and concentration of surfactants was studied. It was noted that using Pluronic F127, by increasing its concentration, the size of the SLNs improved, while with Pluronic F68 and poly(vinyl alcohol) (PVA), the trend was the opposite. Instead, Pluronic F68-based SLNs formed smaller particles than PVA and Pluronic F127. The best combination of parameters was proved to be the one involving the surfactant F68 at 2% w/v, with a flow rate of 5 : 15, fabricating SLNs with a diameter of ~180 nm and a PDI value of ~0.23. Clearly, device 2 can fabricate smaller SNLs by means of its higher mixing efficiency. Moreover, by additionally decreasing the lipid concentration up to 10 mg ml^{-1}, the diameter further decreased to 178 nm, keeping the same PDI. Subsequently, SLNs were loaded with sorafenib (SFN) and paclitaxel (PTX) drugs for cancer therapy. The drug loading (DL) and encapsulation efficiency (EE) were evaluated: the PTX-SLN best drug concentration was seen to be 0.75 mg mL^{-1}, with an EE of 54% and a DL of 1.4%. While for SFN-SLNs, the best concentration was found to be 0.5 mg mL^{-1} with an EE of 79% and a DL of 1.04%. Besides polymer-based NPs, LNPs and SLNPs have been used as effective carriers for a variety of anticancer drugs. However, there are still some challenges such as the chip design and drug encapsulation efficiency; the latter represents a key issue if the scientific community wants to use microfluidic-based NPs as carriers for cancer treatment. For this reason, in the next few years the direction of research, in our opinion, should be focused on the uses of herringbone staggered micromixer chips that can lead to both high drug encapsulation efficiency and possible industrial scalability.

3.3. Structured nanoparticles

The development of lipid-based and polymer-based nanocarriers was reported to be an advantageous approach of designing novel and more efficient carriers for targeting and controlling drug release.[121,122] In this context, the preparation of lipid–polymer hybrid nano-systems (LPHNSs) has emerged as a valuable strategy to overcome some of the drawbacks that lipid nanosystems (high polydispersity, low biphasic release, physicochemical and biological stability) and polymer nanosystems (reduced drug loading and encapsulation efficiency) exhibit taken individually.[123] As well as other kinds of nanocarriers, in the last few years the introduction of MMs allowed overcoming some problems that traditionally affect BMs for the preparation of LPHNSs.[124] In this paragraph are reported examples of microfluidic chips optimized to design single-step processes for the fabrication of LPHNSs,[125] or to prepare LPHNSs with microscopic architectures that would be inaccessible through traditional BMs.[126] LPHNSs for drug release based on PLGA and 1,2-distearoyl-*sn-glycero*-3-phosphoethanolamine-*N*-[methoxy(polyethylene glycol)-2000] (DSPE-PEG2000) were prepared by co-flow nanoprecipitation.[125] The microfluidic chip was fabricated with borosilicate glass capillaries, to obtain a device resistant to organic solvents. LPHNSs were loaded with the anticancer drug sorafenib (SFN), a model drug, and were compared with LPHNSs prepared with

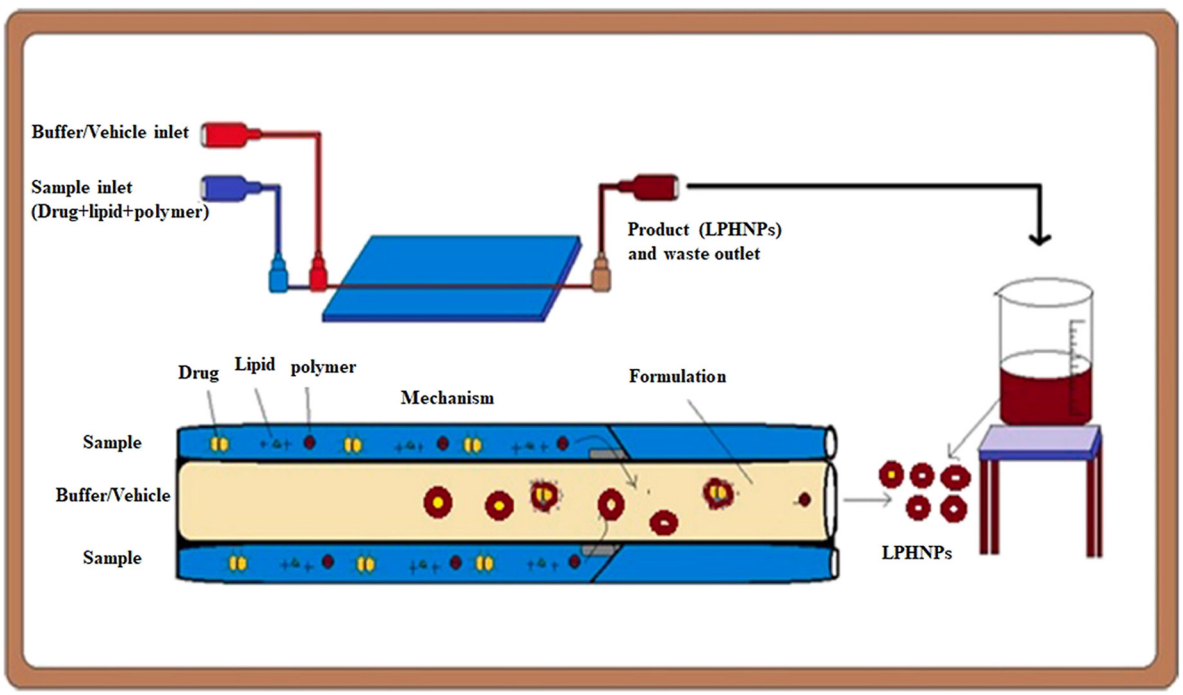

Fig. 9 Scheme of the setting of the microfluidic apparatus and of the LPHNS fabrication. Reprinted with permission from ref. 125. Copyright 2020. Elsevier.

the nanoprecipitation BM. A PLGA acetonitrile solution (inner fluid) and a lipid ethanol solution (outer fluid) were injected into the microfluidic system by means of syringe pumps at an inner/outer flow rate ratio from 1 : 5 to 1 : 50 mL h^{-1}. The microfluidic system and the LPHNS preparation process are schematized in Fig. 9.

The size (320–191.8 nm) and the PDI (0.163–0.1) of LPHNSs prepared with the microfluidic method were found to decrease as the ratio decreased, resulting in more sensitivity to the fabrication conditions compared to the size (~200 nm) and PDI (~0.2) of LPHNSs prepared with the BM. The drug encapsulation efficiency of the microfluidic-prepared LPHNSs (88–95%) resulted in higher and more sensitivity to fabrication conditions than that obtained from the BM (88–89%). The size, PDI and ζ potential of the microfluidic-prepared LPHNSs were stable over 10 days in three different media (PBS, RPMI, DMEM). LPHNSs fabricated with the microfluidic system exhibited a controlled release of the drug over 24 h, and were tested *in vitro* with breast cancer (MDA-MB-231) and prostate cancer (PC3) against which the NPs showed higher anticancer activity compared to the bulk method prepared NPs. Core–shell NPs based on polyethylenimine-*graft*-polycaprolactone (PCL-PEI) and lipids were prepared by means of a three-stage microfluidic chip for the delivery of small interfering RNA (siRNA).[26] siRNA is deeply studied in the literature as a therapeutic agent against different kinds of degenerative and chronic diseases,[126–128] but requires a suitable carrier to be administered, as it easily undergoes enzymatic degradation (RNAses) and elimination by kidneys. Traditionally nano-systems for the delivery of siRNA are prepared by means of BMs that involve the compaction of siRNA into nanoplexes by using cationic surfactants. These nanostructures showed a premature release of siRNA into the bloodstream, causing an immunogenic reaction. They also were proved to be directly toxic due to the residual positive charge. A MM was proposed for the production of core–shell NPs in which siRNA is enclosed in PCL-PEI reverse micelles, which are surrounded by a lipid neutral membrane. The microfluidic chip was specially designed for the fabrication of lipid/PCL-PEI/siRNA (LPS) NPs, with five inlets, two straight mixing channels, one double spiral mixing region and one outlet. The injection of all components was controlled by syringe pumps. The siRNA water solution was injected in the middle inlet, and at the first junction of the chip, it was mixed with a solution of PCL-PEI in DMSO, injected from the peripheral inlet. In this stage, PCL-PEI/siRNA complexes, due to the interaction between the cationic PEI moiety and the anionic siRNA, were formed. Two water streams were injected into the two side inlets, and they were mixed with the central flow at the second junction. In this stage, the PCL-PEI/siRNA was forced to arrange in reverse micelles because of the solvent-switching effect of DMSO/water. The water suspension of reverse micelles was stabilized by mixing at the third junction with the lipid solution in ethanol, containing cholesterol, DSPE-PEG2000 and 1,2-dioleoyl-*sn-glycero*-3-phosphoethanolamine (DOPE). The lipid solution was injected through the middle inlet. The final NP suspension was collected at the exit from the outlet. LPS was compared with lipid/micelle/siRNA (LMS) prepared using the same components. PEI-PCL micelles were prepared by means of the thin-film hydration method, mixed with siRNA and then coated with lipids. The microfluidic process and the comparison of *in vivo* transport of LPS and LMS are reported in Fig. 10.

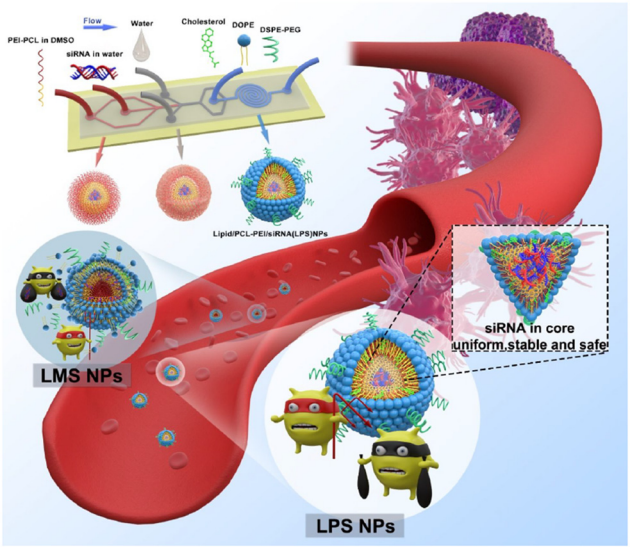

Fig. 10 Representation of the microfluidic process and comparison of *in vivo* circulation of LPS and LMS. Reprinted with permission from ref. 26. Copyright 2020. American Chemical Society.

The size of LPS was smaller (d ~ 120 nm) than that of LMS (d ~ 200 nm), with a narrower PDI and greater size stability over 14 days. Furthermore, the microfluidic method produced NPs with a more negative zeta potential (−8.8 mV LPS, −1.2 mV LMS) and higher encapsulation efficiency (LPS 98%, LMS 79%). Finally, LPS exhibited improved biological features, with evident downregulation of the estimated glomerular filtration rate (eGFR) mRNA and of the protein expression level, and improved action against human prostate cancer PC-3, tested *in vitro* and *in vivo*. The Tesla mixer is another microfluidic architecture, composed of repeating units of channel diversions and it blends for a rapid mixing widely used to fabricate lipid-based NPs (Fig. 11).

The Tesla mixer was employed to fabricate in a single step hybrid lipid–polymer NPs by nanoprecipitation; in particular, the central stream consisting of PLGA solubilized in acetonitrile focused between lipid streams consisting of lecithin and lipid–PEG in water. By varying the polymer and lipid, or functionalizing the lipid reagents, different NP sizes (35–180 nm), charge (−10 to +20 mV), and stability were observed which could be applicable for drug delivery in the cancer therapy field.[129] Generally, the one-step MMs are favored compared to the two-step method thanks to their simplicity; moreover, the crucial parameter in order to

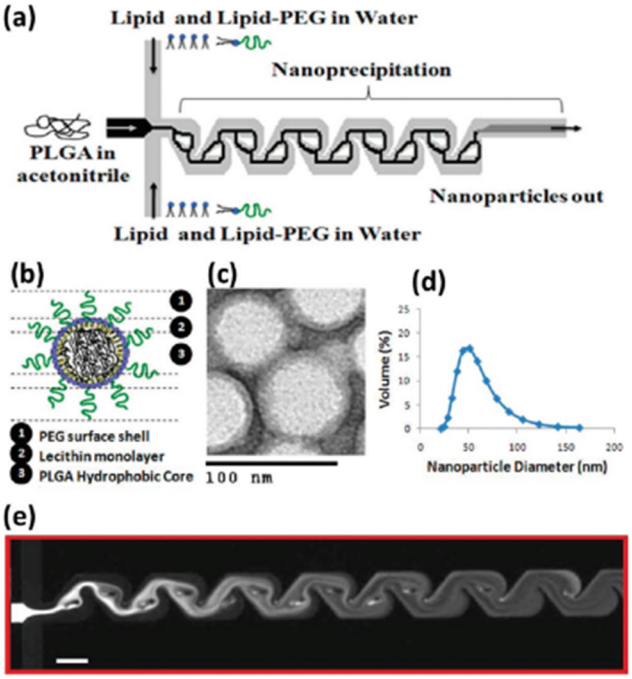

Fig. 11 Nanoprecipitation of lipid–polymeric NPs: (a) schematic representation of Tesla structures for the production of hybrid lipid–polymeric NPs, (b) figure of a NP. (c) TEM image of NPs, (d) average size distribution of NPs $d \sim 40$ nm. (e) Solvent mixing in the Tesla micromixing structures with a scale bar of 100 μm. Reprinted with permission from ref. 129. Copyright 2010. American Chemical Society.

achieve the control of physicochemical properties, drug encapsulation efficiency and the release kinetics of NPs is based on the lipid–polymer ratio and the colloidal stability due to steric hindrance provided by polymer chains. Furthermore, even if the emulsification–solvent evaporation method (ESEM) represents one of the best methods to produce these nanosystems, great efforts have been and will be made to shift to the one-pot nanoprecipitation method that can provide higher drug encapsulation efficiency, as reported in Table 1, and industrial scalability compared to the ESEM.

3.4. Inorganic-based nanoparticles

Inorganic-based NPs are widely used in a variety of fields, such as optoelectronics,[130] imaging,[131] sensing,[132] catalysis[133] and especially in the drug delivery field,[134] due to their unique physicochemical properties on the nanoscale. Thanks to the advantages mentioned above, microfluidic technologies have been widely employed for the fabrication and surface modification of inorganic nanomaterials, such as metal and metal/metal composite NPs,[135] silica NPs,[136] metal–organic frameworks (MOFs)[137] and quantum dots (QDs).[138] In particular, in the synthetic procedure, the monodispersity of inorganic-based NPs is completely dependent on the reaction kinetics, their mixing, the reaction fluids, and the temperature. All these features are precisely controlled in microfluidic devices.[139] The inorganic-based

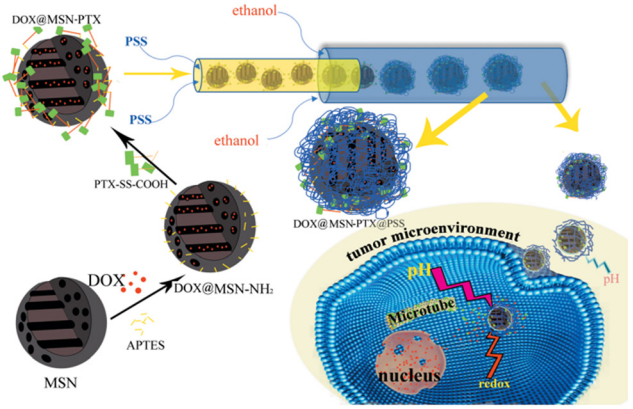

Fig. 12 Fabrication of DOX-loaded MSN-PTX/PSS by means of microfluidics. The PSS layer swells under an acidic tumor microenvironment; thus, the MSN becomes positively charged and can be internalized by tumor cells *via* endocytosis. Yan J. *et al.*[141]

NPs are non-toxic, biocompatible, hydrophilic, and highly stable and are widely employed for the design of new drug delivery systems in order to enhance target efficiency to the cancer cells and reduce adverse effects.[140] Some examples, reported in the literature in the last two years, based on inorganic-based NPs have been selected and described as follows. A pH/redox-triggered mesoporous silica nanoparticle (MSN)-based nanoplatform has been fabricated for DOX/paclitaxel (DOX/PTX), in which PTX is covalently linked to the DOX-loaded MSNs through a disulfide bond. This modification has been applied for two reasons: i) to improve the PTX loading and ii) PTX and the linker act as a redox-sensitive gateway to control the release profile of both drugs. Afterward, polystyrene sulfonate (PSS) is coated onto DOX-loaded MSN-PTX in a 3D microfluidic co-current focusing device, Fig. 12, using two miscible liquids (ethanol and water) which are injected into the microfluidic device separately, by electrostatic interaction to become acidic pH-responsive and to neutralize the ζ potential in order to reduce the non-specificity endocytosis of healthy cells. The diameter d of DOX-loaded/MSN/PTX/PSS NPs was ~148.93 nm.

In vitro cytotoxicity assays performed on cancer cell BT549 and healthy breast cell MCF-10A, showed that the NPs can selectively release DOX and PTX and eliminate cancer cells with a negligible effect on the healthy breast cells, thanks to the acidic microenvironment in cancer cells.[141] Hao *et al.* developed a simple strategy to fabricate ellipsoidal mesoporous silica nanomaterials (EMSNs) with ordered parallel channels employing cetyltrimethylammonium bromide and tyrosine as structure-directing agents and tetraethyl orthosilicate as a silica precursor in dilute ammonia solution. In order to produce the hollow counterparts of EMSNs employing phosphate-buffered saline (PBS) as the etching agent and bovine serum albumin (BSA) protein as the surface protective coating, a miniaturized microfluidic device with spiral-shaped channels was used and is reported in Fig. 13.

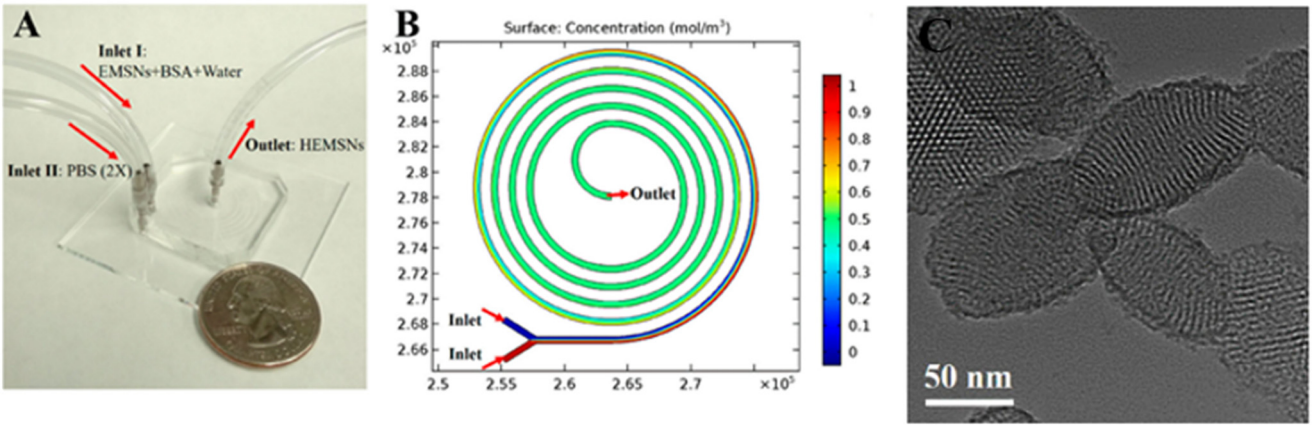

Fig. 13 A) Microfluidic chip for the fabrication of EMSNs. (B) COMSOL simulation result of mixing in the microfluidic spiral channel, and their morphologies. Reprinted from ref. 142.

The microfluidic device was composed of a five-run spiral microchannel with two inlets for mixing the reactants and one outlet for collecting the resultant nanomaterials. Briefly, EMSNs and BSA protein were dispersed in water as one inlet flow and an equivalent volume of PBS as the other inlet flow. Subsequently, DOX was loaded by mixing with nanomaterials under stirring under dark conditions. Cytocompatibility assays showed that DOX-loaded EMSNs had low cell viability of SK-BR-3 compared to unloaded EMSNs.[142] Li *et al.* developed sub-10 nm organic aggregation-induced emission (AIE) particles using four different AIE luminogens (AIEgens) with emissions from green to the second near-infrared window (NIR-II). The AIE QDs were synthesized *via* nanoprecipitation by means of a microfluidic chip composed of three inlets, a mixing channel and a double spiral mixing channel and one outlet (Fig. 14a).

Subsequently, the fluorescence emission of these AIEgens ranges from green to NIR-II, including the four reported AIEgens 4,7-bis[4-(1,2,2-triphenylvinyl)phenyl]benzo-2,1,3-thiadiazole (Bt), 4,7-bis(4-(1,2,2-triphenylvinyl)phenyl)-spiro[benzo-[*d*]imidazole-2,1′-cyclohexane] (Bi), 2,3-bis(4-(phenyl(4-(1,2,2-triphenylvinyl)phenyl)amino)phenyl) fumaronitrile (Fn), and 4,7-(bis4-(4-octylthiophen-2-yl)-*N*,*N*-diphenylaniline)benzo[1,2-*c*:4,5-*c*′]bis([1,2,5]thiadiazole) (Ttb), which are synthesized as reported elsewhere.[142–145] Thanks to microfluidic mixing, the hydrophobic fatty acid chains of amphipathic Dspe-PEG2k can link to the aggregated hydrophobic AIE core and the hydrophilic PEG chains allow the QDs to be soluble in aqueous solutions. These AIE dots, produced by a microfluidic chip, show quantum size and their name was AIE quantum dots (QDs) in order to distinguish them from the normal AIE dots with a diameter >25 nm. In particular, the quantum size effects, >25 nm, are significant for the biological properties. Indeed, the AIE QDs lead to more efficient cell internalization and imaging without surface modification using any membrane-penetrating peptides than AIE dots. They demonstrated that the AIE QDs with NIR-II fluorescence could improve the tumor-targeting compared to >25 nm AIE dots and evasion from the liver. Moreover, NIR-II AIEgens have been employed to demonstrate that AIE QDs can achieve high contrast at the tumor as small as 80 mm^3 (Fig. 13B) and evade the liver more efficiently than AIE dots. AIE QDs hold to offer the possibilities for precise diagnosis of the solid tumor in clinical medicine with much lower off-targeting to the liver than AIE dots.[146] Balachandra *et al.* developed an integrated microfluidic chip to synthesize an aptamer-modified biozeolitic imidazolate framework (BioZIF-8) to target the lymph nodes and tumor. Briefly, the microfluidic chip was composed of a three-spiral mixing channel to synthesize

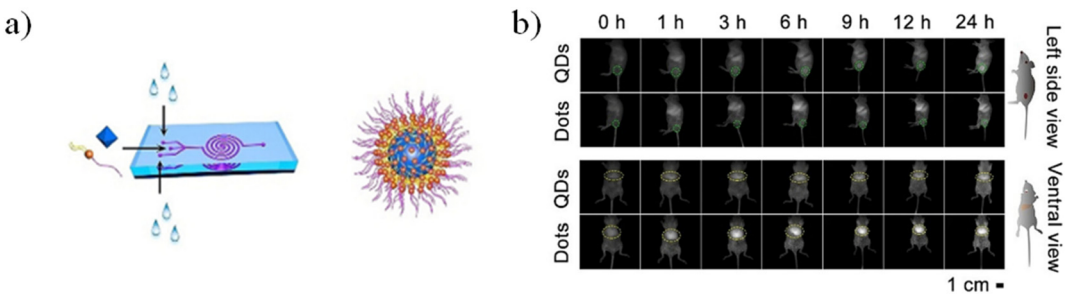

Fig. 14 a) Microfluidic fabrication of AIE QDs and the structure of AIE QDs. b) NIR-II fluorescence images of 4T1 tumor bearing mice treated with Ttb QDs or Ttb dots for 24 h from the side view and the ventral view. Green circles indicate the tumor. Yellow circles indicate the liver. Reprinted with permission from ref. 146.

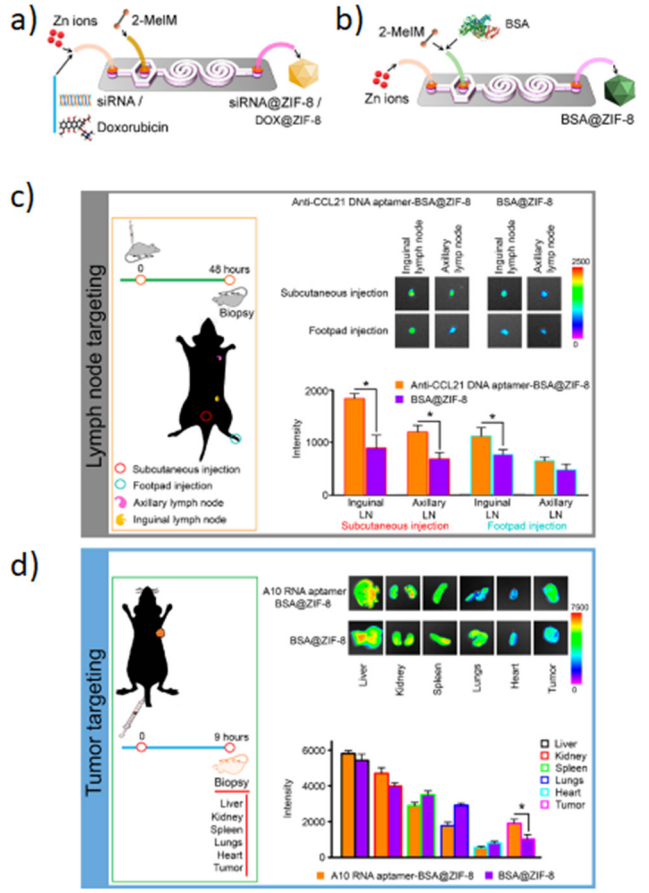

Fig. 15 The microfluidic chip for the fabrication of: a) BioZIF-8, b) siRNA-ZIF-8 and DOX-ZIF-8 MOFs; c) and d) aptamer-functionalized BSA–ZIF-8 targets the lymph node and tumor. Reprinted with permission from ref. 149. Copyright 2021. American Chemical Society.

ligand-functionalized BioZIF-8 in two steps (Fig. 14a). The first step the ZIF-8 was synthesized, in which ZIF-8 encapsulating biomolecules (bovine serum albumin, small interfering ribonucleic acid, and DOX), while in the second step, the BioZIF-8 was MOFs surface-functionalized with two different aptamer ligand, RNA aptamer and DNA, in order to target the lymph nodes and tumor. In particular, the anti-CCL21 DNA aptamer targets the chemokine ligand 21 of a cytokine in the T cell-rich region of lymph nodes, while to target the tumor, an A10 RNA aptamer is employed.[147] The A10 RNA aptamer recognizes the extracellular domain of the prostate-specific membrane antigen (PSMA) on the surface of prostate cancer cells.[148] The preparation of the aptamer functionalized BioZIF-8 MOFs employing a one-step, one-chip microfluidic approach is reported in Fig. 15a.

The *in vivo* evaluation was aimed at evaluating the targeting efficiency of aptamer-functionalized BSA–ZIF-8 MOFs to the lymph nodes (Fig. 15c) and tumor in a mouse model (Fig. 15d). The targeting efficiency from the lymph nodes showed a significant increase for the anti-CCL21 DNA aptamer–BSA–ZIF-8 MOF-treated mice compared to those without an aptamer as well as the zinc concentration (Fig. 15c). Furthermore, also in the case of prostate cancer cells, the targeting efficiency was higher for A10 RNA aptamer-functionalized FITC–BSA–ZIF-8 MOFs than those unfunctionalized. According to the targeting efficiency data, the tumor data show a higher accumulation in the tumor when the mice are treated with A10 RNA aptamer–BSA–ZIF-8 MOFs than those without an aptamer (Fig. 15d). These data are also consistent with the zinc concentration for the A10 RNA aptamer–BSA–ZIF-8 MOF-treated mice.[149] Although in recent years scientific research has been focused on different types of inorganic NPs, *i.e.* QDs, silica, metal/composite NPs and MOFs, the microfluidic-based synthetic strategies of inorganic NPs present some drawbacks such as the low control of the synthetic mechanism, the liquid evaporation related to the high temperature achieved during the synthetic procedures, the low yield that until now stops at grams per hour, the morphology modulation and industrial production. In order to improve the drawbacks mentioned above, computational and predictive analyses for an integrated design methodology of new chips can be an effective strategy to develop inorganic NPs with precise control of the synthetic mechanism and in order to achieve nanocarriers with high performances. Furthermore, a hotplate adapter for the chips was developed with dolomite in which the chip is located between two plates hermetically sealed in order to avoid solvent evaporation. Based on these findings, in the future, with the rapid development of microfluidic technologies, based on the design of the new chips, a wide set of functional inorganic NPs, with controlled synthetic mechanisms and physicochemical properties such as shape and size, are expected to be realized in order to develop new nanocarriers for cancer treatments.

3.5. Metal-based nanoparticles

Metal-based nanoparticles (MNPs) composed of pure metals, such as Fe,[150,151] Co,[151] and Ni,[152] or composed of alloys, such as FePt,[153] NiPt,[154] and NiPd,[155] were fabricated for hyperthermia application thanks to their magnetic properties. Ferromagnetic nano-sized NPs exhibit superparamagnetic behavior, presenting a single magnetic domain.[156] Under an external alternating magnetic field, these magnetic NPs quickly reoriented their magnetic moment, leading to a loss of energy that can be used to heat the surrounding tissues and locally destroy tumor cells.[157] Once the magnetic field is removed, the NP net magnetic moment vanishes and the NPs act like a non-magnetic material.[158] Nevertheless, there are some limitations associated with the use of MNPs, because of their tendency to aggregate and precipitate when they are introduced into the blood vessels, leading to low stability and biocompatibility.[159] To overcome these issues, MNPs are often covered with an organic biocompatible coating, generating metal–organic nanoparticles (MONPs).[160] Furthermore, MNPs and MONPs can be loaded with anticancer drugs for cancer treatment and used as nanocarriers characterized by high versatility and high drug

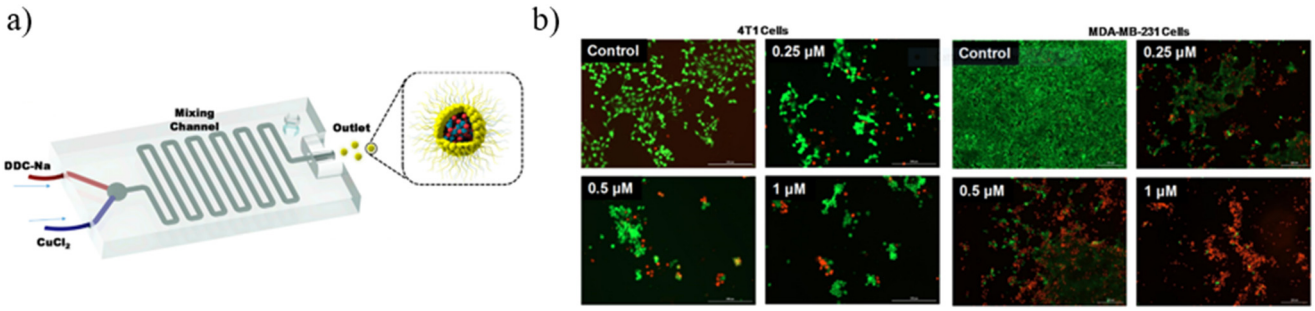

Fig. 16 (a) Schematic illustration of the mixing microfluidic device adopted to fabricate BSA/Cu(DDC)$_2$ MONPs. (b) MTT assay results of 4T1 cells and MDA-MB-231 cells treated with BSA–Cu(DDC)$_2$ for 48 hours. Reprinted with permission from ref. 162. Copyright 2019. Elsevier.

delivery efficiency.[161] Some examples describing MNPs fabricated by microfluidic devices are described as follows. Biomimetic diethyldithiocarbamate copper (Cu(DDC)$_2$) NPs superficially decorated with bovine serum albumin (BSA) were prepared for breast cancer therapy by using a 3D-printed microfluidic device. The precise control of the mixing process and massive production can be achieved, leading to easy clinical translation and future commercialization. The BSA employment on the NP surface is crucial for NP stabilization because it can act as a targeting ligand to bind with some proteins (SPARC receptors) overexpressed by tumor cells. For this experiment, a mixing microfluidic device was prepared with a 3D printer (Creality CR-10) using PLA as a printing material. Briefly, BSA/Cu(DDC)$_2$ NPs were prepared by dissolving sodium diethyldithiocarbamate trihydrate (DDC-Na) and copper chloride ($CuCl_2$) with two BSA containing aqueous solutions at 1% w/v concentration, respectively. Then, DDC-Na and $CuCl_2$ solutions were injected into the microfluidic device through two inlets by a syringe pump (Fig. 16a). Different experiments were conducted at different flow rates (0.5, 1, 2 ml min^{-1}) and the molar ratio between DDC-Na and $CuCl_2$ solutions was fixed to 2 : 1.

The outlet solution containing MONPs was purified by centrifugation and subsequent filtration. The use of the microfluidic mixer device allows for obtaining NPs with a size of around 65 nm, a PDI of around 0.2 and a ζ potential of around −30 mV, because of the presence of BSA covering the NP surface. Furthermore, thanks to the BSA stabilizing action, the NP size remains constant over the first 60 hours. The enhanced mixing efficiency guaranteed by microchannels leads to a high yield of NP production (95%). The loaded drug percentage is a function of the flow rate into the device microchannel. Indeed, by increasing the flow ratio from 0.5 ml min^{-1} to 2 ml min^{-1}, the drug concentration in

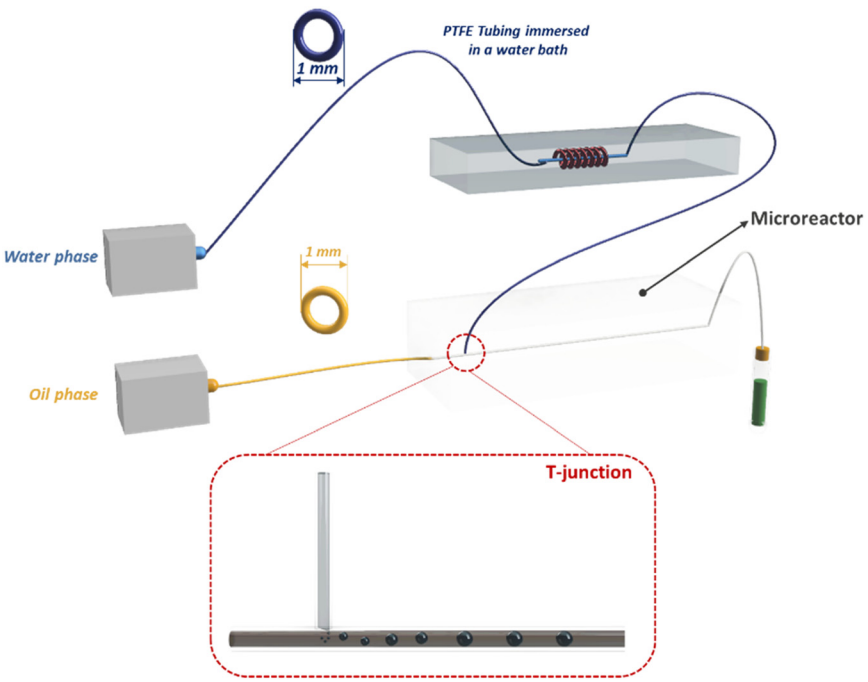

Fig. 17 Experimental setup for fabrication of CpE loaded CS NPs.

the MONPs increases from 1.3 mg ml^{-1} to 1.9 mg ml^{-1} and the drug loading percentage increases from 66% to 95%, thanks to the better mixing efficiency that the mixing microdevice has when the flow rate becomes higher. Moreover, the microfluidic device developed for these experiments allows for increasing the NP production rate, managing to fabricate 240 ml of BSA/$Cu(DDC)_2$ NPs (2 mg ml^{-1}) per hour. Finally, *in vitro* experiments were performed to test the BSA/$Cu(DDC)_2$ antitumor activity. For a drug concentration of 1 μM, after 48 hours MTT tests showed a cell viability of around 20% for MDA-MB-231 cells and of 0% for 4T1 cells (Fig. 16b).[162] A polymethyl-methacrylate (PMMA) microfluidic chip was employed to fabricate silver nanocarriers embedded by CS and loaded with a *Calotropis procera* extract (CpE), which seems to have biological properties, among which is anti-cancer activity. Chitosan/silver NPs (CS NPs) were fabricated by means of a T-junction microreactor device reported in Fig. 17.

The continuous oil phase (canola oil) was fluxed through the straight channel by means of a syringe pump. The dispersed aqueous phase (reaction mixture) was prepared by mixing 1.5% of CS solution and a 4 mM $AgNO_3$ solution at a volumetric ratio of 4 : 1, respectively. 40 mg of CpE was dissolved in a polar solvent (2 : 3, ethanol : dH_2O) and it was added to an aqueous solution at different volumetric ratios (1, 2, 4 and 6). The reaction mixture was heated by flowing through a helically coiled polytetrafluoroethylene (PTFE) tube immersed in a temperature-controlled water bath at 90 °C. The reaction mixture heating is crucial to activate the effective capping efficiency of CS on silver. After the reaction mixture was injected through the perpendicular channel to form the microemulsion, which was collected at the outlet of the chip, for some samples, 10% of NaOH was added into the sample for further reduction. The CS NPs obtained were centrifuged and the resulting NPs were lyophilized for subsequent analysis. The SEM micrographs showed different morphologies between loaded and unloaded CS NPs. Indeed, unloaded CS NPs revealed an irregular shape with a rough surface, probably due to some agglomeration of silver NPs. Meanwhile, silver NPs were quite visible on the smooth surface of CS and CpE, after CpE loading. This difference could be interpreted considering that CpE has a significant role in determining and stabilizing NP surfaces. Therefore, SEM analysis pointed out that samples fabricated without the reaction mixture heating showed a completely different morphology (flower-like), consisting of interconnected nano-needles of Ag_2O with a mean diameter of 161 ± 25 nm. The drug encapsulation efficiency was found to be higher for heated samples (77%) than for samples fabricated at room temperature (57%), thanks to the better encapsulation efficiency of CA NPs compared to the Ag_2O nano-needles. H_2O_2 antioxidant assays were conducted to evaluate the CA NP antioxidant activity. The scavenging ability of CpE CS-2 NPs (CpE loaded CS NPs in which CpE was added to the reaction mixture at a volumetric ratio equal to 2) was higher as compared to that of free CpE at low concentration, thus the presence of CS microcarriers increases the CpE scavenging proficiency. Finally, *in vitro* assays were performed to evaluate the antitumor activity of loaded CS NPs against 4T1 cells and demonstrated that CS NPs increase the cytotoxicity of free CpE. In particular, CpE CS-2 NPs showed better results in terms of cytotoxicity, reducing the cell viability up to 6.34% and 4.63% at concentrations of 80 μg ml^{-1} and 100 μg ml^{-1}, respectively, after 24 hours.[163] Despite the numerous advances made in the fabrication of MNPs through microfluidics,[164] great efforts should be made to simplify the MNP fabrication and improve their drug encapsulation efficiency as well as physicochemical property control in order to be efficient nanocarriers used in cancer therapy. An effective strategy, to overcome these drawbacks, could be based on: 1) the design of simple chips, supported by computational modeling and 2) the employment of real-time characterization in order to monitor all variations during the MNP structure formation. Therefore, with the use of new chip designs, it could be possible to achieve nanocarriers with high drug encapsulation efficiency and high morphology control in order to achieve their fast industrial scalability.

4. Conclusions and future perspectives

We have highlighted some of the most important microfluidic technologies employed for the production of NPs; in particular, the microfluidic platform offers a higher level of control of physicochemical properties, such as size, shape and morphology, in the production of nanoparticles than the conventional fabrication methods. The precise control of the physicochemical properties is a key parameter to design and develop new technology platforms for the development of drug delivery systems for cancer therapy. Indeed, the success of microfluidic technology is based on: (i) rapid mixing in microfluidic channels in order to obtain monodisperse nanoparticles with a high yield; (ii) the precise control of physicochemical properties to obtain batch-to-batch reproducibility; (iii) the integration of multiple fabrication procedures in a single microfluidic device to allow for the fabrication of nanoparticles with desired structures in one step. Microfluidic devices, with all these features, represent an ideal system for controllable fabrication and practical applications of a variety of nanoparticles. Although many efforts have been made in the last decade, it is clear from the current state of the art of microfluidic research for NP fabrication that not all drug delivery systems can be used for cancer treatments due to the low drug encapsulation efficiency or due to the not easy up-scalability to the industrial scale. Therefore, in order to face the drug load capacity and frequent drug expulsion, different types of enhancements such as 1) the choice of the raw materials such as the production of nanoparticles without any chemical modifications, 2) the one-pot synthesis and 3) the design of the chips must be considered. Indeed, the design of *ad hoc*

microfluidic device architectures can improve both the drug encapsulation efficiency and the production rates of NPs. For instance, a device composed of parallel channels or several mixing chambers can be used as an effective strategy to improve industrial scalability. However, although the employment of microfluidic devices for nanoparticle fabrication is still under great exploration, research carried out in the last two decades, especially in the last five years, has demonstrated that microfluidics could facilitate the fabrication of nanoparticles for cancer therapies. Currently, the use of many NP-based materials in experimentation on animal models is stopped, but the new opportunities provided by microfluidics represent the possibility to move forward with the clinical translation. Thanks to the new advancements that are occurring in the design of both microfluidic technologies and nanomaterials, fabricated with microfluidics, the research activity, in this field, will inevitably provide new ideas in the future for producing new functional nanomaterials applicable in the cancer therapy field.

Author contributions

All authors contributed to the writing, discussion, and correction of this perspective.

Conflicts of interest

The authors declare no competing financial interest.

Acknowledgements

The authors acknowledge the research project "ADViSE: Antitumor Drugs and Vaccines From The Sea"-Por Campania FESR 2014–2020 with the AXIS 1 OO.SS. 1.2.2/1.1 CUP B43D18000240007.

References

1 P. Couvreur, *Adv. Drug Delivery Rev.*, 2013, **65**, 21–23.
2 M. J. Mitchell, M. M. Billingsley, R. M. Haley, M. E. Wechsler, N. A. Peppas and R. Langer, *Nat. Rev. Drug Discovery*, 2021, **20**, 101–124.
3 A. Bokare, A. Takami, J. H. Kim, A. Dong, A. Chen, R. Valerio, S. Gunn and F. Erogbogbo, *ACS Omega*, 2019, **4**, 4650–4657.
4 S. Abalde-Cela, P. Taladriz-Blanco, M. G. de Oliveira and C. Abell, *Sci. Rep.*, 2018, **8**, 2440.
5 K. Cho, X. Wang, S. Nie, Z. Chen and D. M. Shin, *Clin. Cancer Res.*, 2008, **14**, 1310–1316.
6 M. S. Ricci and W.-X. Zong, *Oncologist*, 2006, **11**, 342–357.
7 K. H. Bae, H. J. Chung and T. G. Park, *Mol. Cells*, 2011, **31**, 295–302.
8 J. Wang, D. Mongayt and V. P. Torchilin, *J. Drug Targeting*, 2005, **13**, 73–80.
9 M. E. Davis, Z. Chen and D. M. Shin, *Nanoscience and technology: A collection of reviews from nature journals*, 2010, pp. 239–250.
10 K. Y. Choi, H. Chung, K. H. Min, H. Y. Yoon, K. Kim, J. H. Park, I. C. Kwon and S. Y. Jeong, *Biomaterials*, 2010, **31**, 106–114.
11 E. Blanco, A. Hsiao, A. P. Mann, M. G. Landry, F. Meric-Bernstam and M. Ferrari, *Cancer Sci.*, 2011, **102**, 1247–1252.
12 O. C. Farokhzad, J. Cheng, B. A. Teply, I. Sherifi, S. Jon, P. W. Kantoff, J. P. Richie and R. Langer, *Proc. Natl. Acad. Sci. U. S. A.*, 2006, **103**, 6315–6320.
13 A. N. Lukyanov, T. A. Elbayoumi, A. R. Chakilam and V. P. Torchilin, *J. Controlled Release*, 2004, **100**, 135–144.
14 S. S. Aleksenko, A. Y. Shmykov, S. Oszwałdowski and A. R. Timerbaev, *Metallomics*, 2012, **4**, 1141–1148.
15 J. D. Byrne, T. Betancourt and L. Brannon-Peppas, *Adv. Drug Delivery Rev.*, 2008, **60**, 1615–1626.
16 V. P. Torchilin, *Adv. Drug Delivery Rev.*, 2006, **58**, 1532–1555.
17 H. Wang, T. Ding, J. Guan, X. Liu, J. Wang, P. Jin, S. Hou, W. Lu, J. Qian and W. Wang, *ACS Nano*, 2020, **14**, 14779–14789.
18 K. H. Lee, G. L. Z. Yang, B. E. Wyslouzil and J. O. Winter, *ACS Appl. Polym. Mater.*, 2019, **1**, 691–700.
19 Y. Liu, G. Z. Yang, D. Zou, Y. Hui, K. Nigam, A. P. J. Middelberg and C. X. Zhao, *Ind. Eng. Chem. Res.*, 2020, **59**, 4134–4149.
20 N. M. Pinkerton, L. Behar, K. Hadri, B. Amouroux, C. Mingotaud, D. R. Talham, S. Chassaing and J. D. Marty, *Nanoscale*, 2017, **9**, 1403–1408.
21 X. C. Cui, J. Wang, X. Y. Zhang, Q. Wang, M. M. Song and J. L. Chai, *Langmuir*, 2019, **35**, 9255–9263.
22 S. Maiz-Fernandez, L. Perez-Alvarez, L. Ruiz-Rubio, R. P. Gonzalez, V. Saez-Martinez, J. R. Perez and J. L. Vilas-Vilela, *Polymers*, 2019, **11**(4), DOI: **10.3390/polym11040742**.
23 S. Y. Lee, E. H. Hong, J. Y. Jeong, J. Cho, J. H. Seo, H. J. Ko and H. J. Cho, *Biomater. Sci.*, 2019, **7**, 4624–4635.
24 R. Z. Wang, Y. Luo, S. H. Yang, J. Lin, D. M. Gao, Y. Zhao, J. G. Liu, X. Y. Shi and X. L. Wang, *Sci. Rep.*, 2016, **6**, 33844.
25 J. Zhao, Z. Y. Wan, C. C. Zhou, Q. Yang, J. X. Dong, X. Song and T. Gong, *Pharm. Res.*, 2018, **35**, 196.
26 W. Wei, J. Sun, X.-Y. Guo, X. Chen, R. Wang, C. Qiu, H.-T. Zhang, W.-H. Pang, J.-C. Wang and Q. Zhang, *ACS Appl. Mater. Interfaces*, 2020, **12**, 14839–14854.
27 H. Patil, X. Feng, X. Ye, S. Majumdar and M. A. Repka, *AAPS J.*, 2015, **17**, 194–205.
28 D. Chen, K. T. Love, Y. Chen, A. A. Eltoukhy, C. Kastrup, G. Sahay, A. Jeon, Y. Dong, K. A. Whitehead and D. G. Anderson, *J. Am. Chem. Soc.*, 2012, **134**, 6948–6951.
29 R. Ciriminna, A. Fidalgo, V. Pandarus, F. Beland, L. M. Ilharco and M. Pagliaro, *Chem. Rev.*, 2013, **113**, 6592–6620.
30 D. Desai, Y. A. Guerrero, V. Balachandran, A. Morton, L. Lyon, B. Larkin and D. E. Solomon, *Nanomed.: Nanotechnol., Biol. Med.*, 2021, **35**, 102402.
31 K. K. Zhai, X. P. Pei, C. Wang, Y. K. Deng, Y. Tan, Y. A. Bai, B. C. Zhang, K. Xu and P. X. Wang, *Int. J. Biol. Macromol.*, 2019, **131**, 1032–1037.
32 A. Fabozzi, F. Della Sala, M. di Gennaro, N. Solimando, M. Pagliuca and A. Borzacchiello, *Polym. Chem.*, 2021, **12**, 6667–6687.

33 N. J. Hao, Y. Nie, Z. Xu, A. B. Closson, T. Usherwood and J. X. J. Zhang, *Chem. Eng. J.*, 2019, **366**, 433–438.
34 T. Baby, Y. Liu, A. P. J. Middelberg and C. X. Zhao, *Chem. Eng. Sci.*, 2017, **169**, 128–139.
35 J. P. Ma and C. W. Li, *Sens. Actuators, B*, 2018, **262**, 236–244.
36 D. R. Reyes, H. van Heeren, S. Guha, L. Herbertson, A. P. Tzannis, J. Ducree, H. Bissig and H. Becker, *Lab Chip*, 2021, **21**, 9–21.
37 E. Sah and H. Sah, *J. Nanomater.*, 2015, **2015**, 794601, DOI: **10.1155/2015/794601**.
38 Q. Feng, L. Zhang, C. Liu, X. Li, G. Hu, J. Sun and X. Jiang, *Biomicrofluidics*, 2015, **9**, 052604.
39 R. Ran, Q. Sun, T. Baby, D. Wibowo, A. P. Middelberg and C.-X. Zhao, *Chem. Eng. Sci.*, 2017, **169**, 78–96.
40 A.-S. Yang, F.-C. Chuang, C.-K. Chen, M.-H. Lee, S.-W. Chen, T.-L. Su and Y.-C. Yang, *Chem. Eng. J.*, 2015, **263**, 444–451.
41 D. Liu, H. Zhang, F. Fontana, J. T. Hirvonen and H. A. Santos, *Lab Chip*, 2017, **17**, 1856–1883.
42 J. P. Martins, G. Torrieri and H. A. Santos, *Expert Opin. Drug Delivery*, 2018, **15**, 469–479.
43 K. V. Sharp and R. J. Adrian, *Exp. Fluids*, 2004, **36**, 741–747.
44 J. Atencia and D. J. Beebe, *Nature*, 2005, **437**, 648–655.
45 K. F. Glass, E. Longmire and A. Hubel, *Int. J. Heat Mass Transfer*, 2008, **51**, 5749–5757.
46 P. Kunal, E. J. Roberts, C. T. Riche, K. Jarvis, N. Malrnstadt, R. L. Brutchey and S. M. Humphrey, *Chem. Mater.*, 2017, **29**, 4341–4350.
47 G. Laffite, C. Leroy, C. Bonhomme, L. Bonhomme-Coury, E. Letavernier, M. Daudon, V. Frochot, J. P. Haymann, S. Rouziere, I. T. Lucas, D. Bazin, F. Babonneau and A. Abou-Hassan, *Lab Chip*, 2016, **16**, 1157–1160.
48 J. Marschewski, S. Jung, P. Ruch, N. Prasad, S. Mazzotti, B. Michel and D. Poulikakos, *Lab Chip*, 2015, **15**, 1923–1933.
49 D. Holzinger and A. Ehresmann, *Microfluid. Nanofluid.*, 2015, **19**, 395–402.
50 J. P. Ma, S. M. Y. Lee, C. Q. Yi and C. W. Li, *Lab Chip*, 2017, **17**, 209–226.
51 A. D. Stroock, S. K. Dertinger, G. M. Whitesides and A. Ajdari, *Anal. Chem.*, 2002, **74**, 5306–5312.
52 A. Olanrewaju, M. Beaugrand, M. Yafia and D. Juncker, *Lab Chip*, 2018, **18**, 2323–2347.
53 T. S. Kaminski and P. Garstecki, *Chem. Soc. Rev.*, 2017, **46**, 6210–6226.
54 H. H. Jeong, D. Issadore and D. Lee, *Korean J. Chem. Eng.*, 2016, **33**, 1757–1766.
55 R. Othman, G. T. Vladisavljevic, H. C. H. Bandulasena and Z. K. Nagy, *Chem. Eng. J.*, 2015, **280**, 316–329.
56 J. Jung, S. C. Cao, Y. H. Shin, R. I. Al-Raoush, K. Alshibli and J. W. Choi, *Microsyst. Technol.*, 2018, **24**, 1071–1080.
57 A. L. R. Costa, A. Gomes and R. L. Cunha, *Exp. Therm. Fluid Sci.*, 2017, **85**, 167–175.
58 A. Fabozzi, R. Vitiello, I. R. Krauss, M. Iuliano, G. De Tommaso, A. Amoresano, G. Pinto, L. Paduano, C. Jones, M. Di Serio and G. D'Errico, *J. Surfactants Deterg.*, 2019, **22**, 115–124.
59 A. Fabozzi, I. R. Krauss, R. Vitiello, M. Fornasier, L. Sicignano, S. King, S. Guido, C. Jones, L. Paduano, S. Murgia and G. D'Errico, *J. Colloid Interface Sci.*, 2019, **552**, 448–463.
60 Z. W. Zhou, H. P. Li, K. K. Wang, Q. Guo, C. Z. Li, H. L. Jiang, Y. Q. Hu, D. Oupicky and M. J. Sun, *ACS Appl. Mater. Interfaces*, 2017, **9**, 14576–14589.
61 D. F. Liu, S. Cito, Y. Z. Zhang, C. F. Wang, T. M. Sikanen and H. A. Santos, *Adv. Mater.*, 2015, **27**, 2298–2304.
62 S. K. Dertinger, D. T. Chiu, N. L. Jeon and G. M. Whitesides, *Anal. Chem.*, 2001, **73**, 1240–1246.
63 Z. Nie, S. Xu, M. Seo, P. C. Lewis and E. Kumacheva, *J. Am. Chem. Soc.*, 2005, **127**, 8058–8063.
64 X. Luo, P. Su, W. Zhang and C. L. Raston, *Adv. Mater. Technol.*, 2019, 1900488, DOI: **10.1002/Admt.201900488**.
65 A. Tiwari, A. Maheshwari, V. M. Rajesh and K. B. Singh, *Chem. Eng. J.*, 2019, **377**, 120602.
66 L. Zha, M. J. Shang, M. Qiu, H. Zhang and Y. H. Su, *Chem. Eng. Sci.*, 2019, **195**, 62–73.
67 K. Shahzad, W. Van Aeken, M. Mottaghi, V. K. Kamyab and S. Kuhn, *Microfluid. Nanofluid.*, 2018, **22**, 104.
68 A. M. Streets and Y. Huang, *Biomicrofluidics*, 2013, **7**, 011302.
69 A. Woźniak, A. Malankowska, G. Nowaczyk, B. F. Grześkowiak, K. Tuśnio, R. Słomski, A. Zaleska-Medynska and S. Jurga, *J. Mater. Sci.: Mater. Med.*, 2017, **28**, 1–11.
70 Y. Huang, T. Han, J. Xuan, H. Xu, Y. Wang and L. Zhang, *J. Micromech. Microeng.*, 2018, **28**, 105021.
71 S. Nawar, J. K. Stolaroff, C. Ye, H. Wu, F. Xin and D. A. Weitz, *Lab Chip*, 2020, **20**, 147–154.
72 Z. Lian, Y. Chan, Y. Luo, X. Yang, K. S. Koh, J. Wang, G. Z. Chen, Y. Ren and J. He, *Electrophoresis*, 2020, **41**, 891–901.
73 G. Tetradis-Meris, D. Rossetti, C. N. Pulido de Torres, R. Cao, G. Lian and R. Janes, *Ind. Eng. Chem. Res.*, 2009, **48**, 8881–8889.
74 G. T. Vladisavljević, N. Khalid, M. A. Neves, T. Kuroiwa, M. Nakajima, K. Uemura, S. Ichikawa and I. Kobayashi, *Adv. Drug Delivery Rev.*, 2013, **65**, 1626–1663.
75 A. Fabozzi, F. Della Sala, M. di Gennaro and A. Borzacchiello, *New J. Chem.*, 2022, **46**, 19763–19772.
76 N. M. Belliveau, J. Huft, P. J. Lin, S. Chen, A. K. Leung, T. J. Leaver, A. W. Wild, J. B. Lee, R. J. Taylor and Y. K. Tam, *Mol. Ther.–Nucleic Acids*, 2012, **1**, e37.
77 H. K. Mandl, E. Quijano, H. W. Suh, E. Sparago, S. Oeck, M. Grun, P. M. Glazer and W. M. Saltzman, *J. Controlled Release*, 2019, **314**, 92–101.
78 J. Riewe, P. Erfle, S. Melzig, A. Kwade, A. Dietzel and H. Bunjes, *Int. J. Pharm.*, 2020, **579**, 119167.
79 X. Zhu, C. Vo, M. Taylor and B. R. Smith, *Mater. Horiz.*, 2019, **6**, 1094–1121.
80 Y. M. Cao, L. Silverman, C. H. Lu, R. Hof, J. E. Wulff and M. G. Moffitt, *Mol. Pharmaceutics*, 2019, **16**, 96–107.
81 M. Russo, P. Bevilacqua, P. A. Netti and E. Torino, *Sci. Rep.*, 2016, **6**, 37906.
82 F. Della Sala, A. Fabozzi, M. di Gennaro, S. Nuzzo, P. Makvandi, N. Solimando, M. Pagliuca and A. Borzacchiello, *Macromol. Biosci.*, 2021, 2100304, DOI: **10.1002/Mabi.202100304**.

83 V. P. Galvan-Chacon, L. Costa, D. Barata and P. Habibovic, *Acta Biomater.*, 2021, **128**, 486–501.
84 R. Zoqlam, C. J. Morris, M. Akbar, A. M. Alkilany, S. I. Hamdallah, P. Belton and S. Qi, *Mater. Sci. Eng. C*, 2021, **127**, 112243.
85 Y. Y. Chai, Y. F. Wang, B. Q. Li, W. Qi, R. X. Su and Z. M. He, *Langmuir*, 2021, **37**, 7219–7226.
86 E. Chiesa, F. Riva, R. Dorati, A. Greco, S. Ricci, S. Pisani, M. Patrini, T. Modena, B. Conti and I. Genta, *Pharmaceutics*, 2020, **12**(3), DOI: **10.3390/pharmaceutics12030260**.
87 M. Ghasemi Toudeshkchouei, P. Zahedi and A. Shavandi, *Materials*, 2020, **13**, 1483.
88 M. Brzezinski, M. Socka, T. Makowski, B. Kost, M. Cieslak and K. Krolewska-Golinska, *Colloids Surf., B*, 2021, **201**, 111598.
89 M. Danaei, M. Dehghankhold, S. Ataei, F. Hasanzadeh Davarani, R. Javanmard, A. Dokhani, S. Khorasani and M. Mozafari, *Pharmaceutics*, 2018, **10**, 57.
90 W. Xu, X. Jiang and L. Huang, *Compr. Biotechnol.*, 2019, 560.
91 M. H. Amer, *Molecular and cellular therapies*, 2014, vol. 2, pp. 1–19.
92 A. Akinc, M. A. Maier, M. Manoharan, K. Fitzgerald, M. Jayaraman, S. Barros, S. Ansell, X. Du, M. J. Hope and T. D. Madden, *Nat. Nanotechnol.*, 2019, **14**, 1084–1087.
93 S. Chen, Y. Y. C. Tam, P. J. Lin, M. M. Sung, Y. K. Tam and P. R. Cullis, *J. Controlled Release*, 2016, **235**, 236–244.
94 S. C. Semple, A. Akinc, J. Chen, A. P. Sandhu, B. L. Mui, C. K. Cho, D. W. Sah, D. Stebbing, E. J. Crosley and E. Yaworski, *Nat. Biotechnol.*, 2010, **28**, 172–176.
95 M. Jayaraman, S. M. Ansell, B. L. Mui, Y. K. Tam, J. Chen, X. Du, D. Butler, L. Eltepu, S. Matsuda and J. K. Narayanannair, *Am. Ethnol.*, 2012, **124**, 8657–8661.
96 P. R. Cullis and M. J. Hope, *Mol. Ther.*, 2017, **25**, 1467–1475.
97 I. V. Zhigaltsev, N. Belliveau, I. Hafez, A. K. Leung, J. Huft, C. Hansen and P. R. Cullis, *Langmuir*, 2012, **28**, 3633–3640.
98 S. J. Shepherd, C. C. Warzecha, S. Yadavali, R. El-Mayta, M.-G. Alameh, L. Wang, D. Weissman, J. M. Wilson, D. Issadore and M. J. Mitchell, *Nano Lett.*, 2021, **21**, 5671–5680.
99 Y. Li, R. J. Lee, X. Huang, Y. Li, B. Lv, T. Wang, Y. Qi, F. Hao, J. Lu and Q. Meng, *Nanomedicine*, 2017, **13**, 371–381.
100 B. Magenheim, M. Levy and S. Benita, *Int. J. Pharm.*, 1993, **94**, 115–123.
101 G. P. Zara, R. Cavalli, A. Fundarò, A. Bargoni, O. Caputo and M. R. Gasco, *Pharmacol. Res.*, 1999, **40**, 281–286.
102 R. Pignatello, A. Leonardi, V. Fuochi, G. Petronio Petronio, A. S. Greco and P. M. Furneri, *Nanomaterials*, 2018, **8**, 304.
103 A. zur Mühlen, C. Schwarz and W. Mehnert, *Eur. J. Pharm. Biopharm.*, 1998, **45**, 149–155.
104 M. M. Billingsley, N. Singh, P. Ravikumar, R. Zhang, C. H. June and M. J. Mitchell, *Nano Lett.*, 2020, **20**, 1578–1589.
105 K. T. Love, K. P. Mahon, C. G. Levins, K. A. Whitehead, W. Querbes, J. R. Dorkin, J. Qin, W. Cantley, L. L. Qin and T. Racie, *Proc. Natl. Acad. Sci. U. S. A.*, 2010, **107**, 1864–1869.
106 W. Mehnert and K. Mäder, *Adv. Drug Delivery Rev.*, 2012, **64**, 83–101.
107 A. J. Domb, *Int. J. Pharm.*, 1995, **124**, 271–278.
108 K. Westesen and B. Siekmann, *Int. J. Pharm.*, 1997, **151**, 35–45.
109 R. Lander, W. Manger, M. Scouloudis, A. Ku, C. Davis and A. Lee, *Biotechnol. Prog.*, 2000, **16**, 80–85.
110 L. B. Peres, L. B. Peres, P. H. H. de Araújo and C. Sayer, *Colloids Surf., B*, 2016, **140**, 317–323.
111 S. Benita, *Submicron emulsions in drug targeting and delivery*, CRC Press, 1998.
112 V. Jenning, A. Gysler, M. Schäfer-Korting and S. H. Gohla, *Eur. J. Pharm. Biopharm.*, 2000, **49**, 211–218.
113 R. B. P. Moura, L. M. Andrade, L. Alonso, A. Alonso, R. N. Marreto and S. F. Taveira, *Eur. J. Pharm. Sci.*, 2022, **168**, 106048.
114 R. L. Ball, K. A. Hajj, J. Vizelman, P. Bajaj and K. A. Whitehead, *Nano Lett.*, 2018, **18**, 3814–3822.
115 A. Albanese, P. S. Tang and W. C. Chan, *Annu. Rev. Biomed. Eng.*, 2012, **14**, 1–16.
116 X. Zhao, F. Bian, L. Sun, L. Cai, L. Li and Y. Zhao, *Small*, 2020, **16**, 1901943.
117 C. Martins, F. Araújo, M. J. Gomes, C. Fernandes, R. Nunes, W. Li, H. A. Santos, F. Borges and B. Sarmento, *Eur. J. Pharm. Biopharm.*, 2019, **138**, 111–124.
118 R. Karnik, F. Gu, P. Basto, C. Cannizzaro, L. Dean, W. Kyei-Manu, R. Langer and O. C. Farokhzad, *Nano Lett.*, 2008, **8**, 2906–2912.
119 N. Kimura, M. Maeki, K. Sasaki, Y. Sato, A. Ishida, H. Tani, H. Harashima and M. Tokeshi, *RSC Adv.*, 2021, **11**, 1430–1439.
120 I. Arduino, Z. Liu, A. Rahikkala, P. Figueiredo, A. Correia, A. Cutrignelli, N. Denora and H. A. Santos, *Acta Biomater.*, 2021, **121**, 566–578.
121 A. Gordillo-Galeano and C. E. Mora-Huertas, *Eur. J. Pharm. Biopharm.*, 2018, **133**, 285–308.
122 S. Indoria, V. Singh and M.-F. Hsieh, *Int. J. Pharm.*, 2020, **582**, 119314.
123 R. Varghese, S. Salvi, P. Sood, B. Kulkarni and D. Kumar, *Colloid Interface Sci. Commun.*, 2022, **46**, 100561.
124 A. Dalmoro, S. Bochicchio, S. F. Nasibullin, P. Bertoncin, G. Lamberti, A. A. Barba and R. I. Moustafine, *Eur. J. Pharm. Sci.*, 2018, **121**, 16–28.
125 N. Tahir, A. Madni, W. Li, A. Correia, M. M. Khan, M. A. Rahim and H. A. Santos, *Int. J. Pharm.*, 2020, **581**, 119275.
126 F. Zahir-Jouzdani, F. Mottaghitalab, M. Dinarvand and F. Atyabi, *J. Drug Delivery Sci. Technol.*, 2018, **45**, 428–441.
127 K. Dua, R. Wadhwa, G. Singhvi, V. Rapalli, S. D. Shukla, M. D. Shastri, G. Gupta, S. Satija, M. Mehta and N. Khurana, *Drug Dev. Res.*, 2019, **80**, 714–730.
128 M. A. Subhan and V. Torchilin, *Transl. Res.*, 2019, **214**, 62–91.
129 P. M. Valencia, P. A. Basto, L. Zhang, M. Rhee, R. Langer, O. C. Farokhzad and R. Karnik, *ACS Nano*, 2010, **4**, 1671–1679.

130 P. C. Mondal, D. Asthana, R. K. Parashar and S. Jadhav, *Mater. Adv.*, 2021, **2**, 7620–7637.
131 J. Nam, N. Won, J. Bang, H. Jin, J. Park, S. Jung, S. Jung, Y. Park and S. Kim, *Adv. Drug Delivery Rev.*, 2013, **65**, 622–648.
132 S. M. Ng, M. Koneswaran and R. Narayanaswamy, *RSC Adv.*, 2016, **6**, 21624–21661.
133 Z. Li, T. Zhuang, J. Dong, L. Wang, J. Xia, H. Wang, X. Cui and Z. Wang, *Ultrason. Sonochem.*, 2021, **71**, 105384.
134 M. Liong, J. Lu, M. Kovochich, T. Xia, S. G. Ruehm, A. E. Nel, F. Tamanoi and J. I. Zink, *ACS Nano*, 2008, **2**, 889–896.
135 J. Shen, M. Shafiq, M. Ma and H. Chen, *Nanomaterials*, 2020, **10**, 1177.
136 D.-Y. Kim, S. H. Jin, S.-G. Jeong, B. Lee, K.-K. Kang and C.-S. Lee, *Sci. Rep.*, 2018, **8**, 1–11.
137 M. Mohammad, A. Razmjou, K. Liang, M. Asadnia and V. Chen, *ACS Appl. Mater. Interfaces*, 2018, **11**, 1807–1820.
138 G.-X. Li, Q. Li, R. Cheng and S. Chen, *Curr. Opin. Chem. Eng.*, 2020, **29**, 34–41.
139 L. L. Li, X. Li and H. Wang, *Small Methods*, 2017, **1**, 1700140.
140 Y. Cao, Y. Xie, L. Liu, A. Xiao, Y. Li, C. Zhang, X. Fang and Y. Zhou, *Phytochem. Rev.*, 2017, **16**, 555–563.
141 J. Yan, X. Xu, J. Zhou, C. Liu, L. Zhang, D. Wang, F. Yang and H. Zhang, *ACS Appl. Bio Mater.*, 2020, **3**, 1216–1225.
142 N. Hao, Y. Nie, A. Tadimety, A. B. Closson and J. X. Zhang, *Mater. Res. Lett.*, 2017, **5**, 584–590.
143 D. Ding, C. C. Goh, G. Feng, Z. Zhao, J. Liu, R. Liu, N. Tomczak, J. Geng, B. Z. Tang and L. G. Ng, *Adv. Mater.*, 2013, **25**, 6083–6088.
144 K. Li, W. Qin, D. Ding, N. Tomczak, J. Geng, R. Liu, J. Liu, X. Zhang, H. Liu and B. Liu, *Sci. Rep.*, 2013, **3**, 1–10.
145 C. Tong, X. Zhong, Y. Yang, X. Liu, G. Zhong, C. Xiao, B. Liu, W. Wang and X. Yang, *Biomaterials*, 2020, **243**, 119936.
146 X. Li, M. Zha, Y. Li, J. S. Ni, T. Min, T. Kang, G. Yang, H. Tang, K. Li and X. Jiang, *Angew. Chem., Int. Ed.*, 2020, **59**, 21899–21903.
147 F. Gu, L. Zhang, B. A. Teply, N. Mann, A. Wang, A. F. Radovic-Moreno, R. Langer and O. C. Farokhzad, *Proc. Natl. Acad. Sci. U. S. A.*, 2008, **105**, 2586–2591.
148 V. Bagalkot, L. Zhang, E. Levy-Nissenbaum, S. Jon, P. W. Kantoff, R. Langer and O. C. Farokhzad, *Nano Lett.*, 2007, **7**, 3065–3070.
149 Y. L. Balachandran, X. Li and X. Jiang, *Nano Lett.*, 2021, **21**, 1335–1344.
150 Y. Gu, M. Yoshikiyo, A. Namai, D. Bonvin, A. Martinez, R. Piñol, P. Téllez, N. J. Silva, F. Ahrentorp and C. Johansson, *RSC Adv.*, 2020, **10**, 28786–28797.
151 J. Verma, S. Lal and C. J. Van Noorden, *Int. J. Nanomed.*, 2014, **9**, 2863.
152 H. Fatima, T. Charinpanitkul and K.-S. Kim, *Nanomaterials*, 2021, **11**, 1203.
153 S. Maenosono and S. Saita, *IEEE Trans. Magn.*, 2006, **42**, 1638–1642.
154 N. Griffete, J. Fresnais, A. Espinosa, C. Wilhelm, A. Bée and C. Ménager, *Nanoscale*, 2015, **7**, 18891–18896.
155 I. Apostolova and J. Wesselinowa, *Solid State Commun.*, 2009, **149**, 986–990.
156 J. Wallyn, N. Anton and T. F. Vandamme, *Pharmaceutics*, 2019, **11**, 601.
157 A. Hervault and N. T. K. Thanh, *Nanoscale*, 2014, **6**, 11553–11573.
158 A. Amarjargal, L. D. Tijing, I.-T. Im and C. S. Kim, *Chem. Eng. J.*, 2013, **226**, 243–254.
159 K. Wu, D. Su, J. Liu, R. Saha and J.-P. Wang, *Nanotechnology*, 2019, **30**, 502003.
160 X. Cai, Q. Zhu, Y. Zeng, Q. Zeng, X. Chen and Y. Zhan, *Int. J. Nanomed.*, 2019, **14**, 8321.
161 R. O. Rodrigues, P. C. Sousa, J. Gaspar, M. Bañobre-López, R. Lima and G. Minas, *Small*, 2020, **16**, 2003517.
162 Y. Chang, J. Jiang, W. Chen, W. Yang, L. Chen, P. Chen, J. Shen, S. Qian, T. Zhou and L. Wu, *Appl. Mater. Today*, 2020, **18**, 100492.
163 A. Aftab, S. Bashir, S. Rafique, T. Ghani, R. Khan, M. Bashir, A. Ehsan, M. I. Khan, A. U. Shah and A. Mahmood, *Appl. Nanosci.*, 2020, **10**, 2281–2293.
164 F. Tian, L. Cai, C. Liu and J. Sun, *Lab Chip*, 2022, **22**, 512–529.